ADDIS ABABA UNVERSITY

SCHOOL OF GRADUATE STUDIES

ELECTRICAL PROPERTIES OF TWO HOURS TREATED 4T1 BREAST CANCER CELLS AND EFFECT OF MAGNETIC BEADS ON IONIZATION OF BT20 BREAST CANCER CELLS USING OPTICAL TWEZEERS.

BY

GUTA KORSA

A THESIS SUBMITTED TO THE DEPARTMENT OF PHYSICS IN PARTIAL FULFILMENT OF THE REQUREMENTS FOR THE DEGREE OF MASTER OF SCIENCE IN PHYSICS (LASER SPECTROSCOPY).

ADDIS ABABA UNVERSITY

SEPTEMBER 2024

ADDIS ABABA UNIVERSITY

PROGRAM OF GRADUATE STUDIES

ELECTRICAL PROPERTIES OF TWO HOURS TREATED 4T1 BREAST CANCER CELLS AND EFFECT OF MAGNETIC BEADS ON IONIZATION OF BT20 BREAST CANCER CELLS USING OPTICAL TWEZEERS.

By

Guta Korsa

Addis Ababa University

Department of Physics

Approved by the Examining Board:

Dr. Endris Mohammed Signature _____

Advisor

Prof. Fekadu Gashaw Signature _____

Examiner

Prof. Teshome Senbeta Signature _____

Examiner

STATEMENT OF THE AUTHOR

I affirm that this thesis is my original work and that I have properly cited all sources used. It is submitted in partial fulfillment of the requirements for the MSc in Physics (Laser Spectroscopy) at Addis Ababa University. I confirm that this thesis has not been submitted to any other institution for any academic degree. Brief quotations from this work are permitted with proper citation. Requests for extended use or reproduction, whether in full or in part, may be granted by the relevant department or the School of Graduate Studies if deemed appropriate for scholarly purposes. All other uses require direct permission from the author.

Name _____ sign_____

Place Addis Ababa University.

Date of submission _____

AKNOWLEDGEMENTS

Above all, I express my heartfelt thanks to God for granting me the opportunity and guidance throughout my life and in the completion of this Thesis. Then I would like to express my gratitude to my instructor, Dr. Endris Mohammed, for his steadfast advice, supervision, and valuable suggestions. His thorough proofreading, insightful comments, and supportive approach have been greatly appreciated. I am also thankful him for his assistance in providing the 4T1 and BT20 breast cancer cells, which were grown and extracted from the Tennessee Center for Botanical Medicine Research's International Ginseng Institute for this study. I am also deeply appreciative of his concern for my well-being, as he regularly checked on my circumstances and provided constant support and encouragement. Additionally, I am thankful Tennessee Center for Botanical Medicine Research's International Ginseng Institute where the cells were cultured and extracted and department of Physics and Astronomy Middle Tennessee State University where the laser trapping experiments were conducted.

During my MSc studies at Addis Ababa University, I had the privilege of meeting many individuals who provided essential support. I would like to extend my deepest appreciation to Prof. Teshome Senbeta, both for his role as my instructor and as the head of the Physics Department, for his unwavering assistance. I am also thankful to my instructors Dr. Lemi D., Dr. Deribe H., Dr. Cherinet A., Dr. Tesgera B., Dr. Belayneh M., and Dr. Kenate N., as well as the advanced lab assistant and the department secretaries. My gratitude also goes to the Dean and Secretaries of the College of Natural and Computational Sciences, and to the staff of the Science and Digital library for their essential support.

Additionally, I would like to thank all my fellow MSc Physics students, especially those in Laser Spectroscopy, Yetwale Alemu, Nigus Birhanu, Gedefow Ayalew, and Ahmed Mohammed, for their support and solidarity in various situations. Finally, I could not have completed this thesis without the support of my father, mother, brothers, sisters, and my wife, Mrs. Alemitu Lamesa.

TABLE OF CONTENT

LISTS OF TABLES

LISTS OF FIGURES

Figure 4.5 shows the charge developed on pre-ionized 2h treated 4T1breast cancer cells versus radius of the cells.

Figure 4.6 shows the relationship between z-number of pre-ionized 2h treated 4T1 breast cancer cells and their angular frequency.

Figure 4.7 shows the data analysis process for measuring the displacement, speed, and time of the BT20 cell using Image pro plus6. The blue dots represent the plotted data points showing the cell movement as it approached and exited the laser trap. The intersection of the yellow x and y lines marks the center of origin. Panel (A) displays the data points recorded before the BT20 cell entered the trap. Panel (B) shows the data points recorded before trapped and after exited the trap.

Figure 4.8 shows the displacement versus time for each of the three selected cells.

Figure 4.9 shows a sequence of snapshots illustrating the cell's trajectory as it moved into, stayed in and subsequently ejected from the trap.

Figure 4.10 illustrates how area of the formed dark region related to time the beads stayed in the trap where area measured is in μm^2 and time is in seconds.

Figure 4.11 illustrates the successive snapshots that show increasing of the brightness with increasing ionization extent of selected BT20 breast cancer cell line as it moved away from the laser trap. The third snapshot (from left to right) shows where the cell is started ejecting and ionizing, and brightness increased rapidly.

Figure 4.12 shows (a) the trajectories of the beads as they ejected from the trap, (b) how the speed of the beads changed over time after ejected from the trap.

LISTS OF ABBREVIATIONS

IARC	International Agency for Research on Cancer
LT	Laser trapping
4T1	Breast cancer cell line of mouse
BT20	Human breast cancer cell line
RT	Radiotherapy
PTX	Pacilitaxel
TCMs	Traditional Chinese Medicines
ROS	Reactive oxygen species
DMDD	2-Dodecyl-6-methoxycyclohexa-2, 5-diene-1, 4-dione
ATP	Adenosine tri-phosphate
PTT	Photothermal therapy
DOX	Doxorubicin
PDT	Photodynamic therapy
PEG	Polyethylene glycol
DCIS	Ductal carcinoma in situ
IDC	Invasive Ductal Carcinoma
ILC	Invasive Lobular Carcinoma
TNBC	Triple-Negative Breast Cancer
OCT	Optical coherence tomography
GNRs	Gold Nano rods
UCNPs	Upconversion nanoparticles
QDs	Quantum dots
CPNPs	Conjugated polymer nanoparticles
NPs	Nano particle

NdYVO4	Neodymium yttrium vanadate laser
$\vec{F}_e$	Electrostatic force
$\vec{F}_d$	Drag force
$\vec{F}_t$	Trapping force
E_0	Electric field amplitude
R_{cell}	Radius of single cell
A_{cell}	Area of single cell
V_{cell}	Volume of single cell
m_{cell}	Mass of single cell
ρ_{cell}	Density of single cell
v_{cell}	Velocity of cell
a_{cell}	Acceleration of cell
v	Speed of light in medium
c	Speed of light in vacuum
μ_0	Permeability of free space
ε_0	Permittivity of free space
A	Beam size calculated
w	Beam radius
PI	Power incident
μ	Viscosity of fetal bovine serum (FBS)
$\vec{r}(t)$	Cells displacement
q	Charge developed on cells
k	Trap coefficient
ω	Angular frequency

ABSTRACT

Study was undertaken to introduce the novel optical tweezers method for exploring the electrical charge developed and trap coefficient of pre-ionized 2 hour treated 4T1 breast cancer cells and to assess how magnetic beads affect the ionization properties of BT20 breast cancer cells. Specifically, the research focused on 4T1 breast cancer cells, which had been treated with the chemotherapy drug DMDD extracted from *Averrhoa carambola L.*, and BT20 breast cancer cells mixed with 3.1 μm diameter polymer-coated magnetic beads. The trapping was achieved using an infrared diode-pumped Nd:YVO4 laser with a wavelength of 1064 nm, maximum output power of 8W, beam diameter of 4 mm, and a highly focused, linearly polarized beam. In experiments with the pre-ionized 2 hour treated 4T1 breast cancer cells, we recorded the following average values; the charge generated on cells in Z-numbers of 432.60±688.77, angular frequency of 72.12±30.12 rad/s and trap coefficient of 8.32±4.55 μN/m. As the cells approached to the center of the trap, their motion was influenced by the opposing of the drag force and the electrostatic force generated by the induced electric field, that resulted in their deceleration. When magnetic beads inserted in BT20 breast cancer cells they affected their ionization characteristics as the cells stayed in the trap.

CHAPTER 1

1. Introduction

Cancer encompasses a range of diseases marked by the uncontrolled proliferation and dissemination of abnormal cells throughout the body, which can lead to death if left untreated. These abnormal cells are referred to as cancer cells, malignant cells, or tumor cells, and they have the ability to invade healthy tissues. Various types of cancers are often named after the tissues from which these abnormal cells originate, such as breast cancer or lung cancer [1]. While the exact causes of cancer development remain largely unclear, several factors are recognized to elevate the risk of developing the disease. These include modifiable factors, such as tobacco use and obesity, as well as non-modifiable factors, like inherited genetic mutations. These risk factors can interact with one another, either simultaneously or sequentially, to initiate and promote the growth of cancer [2].

Cancer continues to be one of the leading causes of death, impacting individuals of all ages across both developed and developing countries. According to recent estimates from the International Agency for Research on Cancer (IARC), there are approximately 12.7 million new cases of cancer reported each year, resulting in 7.6 million deaths globally. A substantial portion of this burden falls on developing countries, where 63% of cancer-related deaths occur [3-5]. Cancer is a complex, multi-genic, and multicellular disease that can originate from various cell types and organs. Its development is influenced by a combination of genetic, environmental, and lifestyle factors. Hanahan and Weinberg [6] identified six key characteristics of cancer, including: cells with unlimited proliferative potential, growth that is independent of the environment, resistance to programmed cell death (apoptosis), the ability to induce angiogenesis (new blood vessel formation), and the capacity for invasion and metastasis to other parts of the body. If uncontrolled cell growth or metastatic spread occurs, it can ultimately lead to the death of the individual [7].

As cancer has many types, breast cancer is one of the most prevalent and aggressive cancer globally and it ranks as the second most common cancer overall cancers. Among women, breast cancer is the most frequently diagnosed cancer and the leading cause of cancer-related deaths. Its high incidence and diverse types make it a major focus of medical research and public health efforts. Breast cancer is a diverse disease with various subtypes, each having distinct characteristics and implications for treatment. The main types of breast cancer cells include ductal carcinoma in situ (DCIS), which is a non-invasive cancer where abnormal cells are confined to the ducts of the breast [8], Invasive Ductal Carcinoma (IDC**)** [9], Invasive Lobular Carcinoma (ILC) which arises from the lobules where milk is produced [10], Triple-Negative Breast Cancer (TNBC) that lacks estrogen receptors, progesterone receptors, and HER2 protein and often more aggressive and harder to treat due to the absence of targeted therapies [11], HER2-Positive Breast Cancer that characterized by overexpression of the HER2 protein, which promotes the growth of cancer cells [12], Luminal A and Luminal B subtypes **(**both subtypes are

estrogen receptor-positive, but Luminal B has a higher proliferation rate and worse prognosis compared to Luminal A**)** [13]**,** 4T1 breast cancer cell [14-15], and BT20 breast cancer cell [16]. 4T1 breast cancer cell is a specific cell line derived from the mammary gland tissue of a BALB/c mouse and BT20 is a human breast cancer cell line derived from a pleural effusion of a patient with breast cancer. Both cell lines are used to study various aspects of breast cancer biology, including metastasis, drug resistance, and tumor microenvironment interactions.

As it reported from the International Agency for Research on Cancer (IARC), over 2.3 million new cases and 685,000 deaths from breast cancer occurred in 2020 [17] and in 2022, there were 2.3 million women diagnosed with breast cancer and 670 000 deaths globally [18]. In our continent Africa, breast cancer continues to be the most commonly diagnosed cancer among women, with incidence rate approximately 50.0 per 100,000 women [19] and mortality rate 27.0 per 100,000 women due to late-stage diagnoses and limited access to advanced treatment [20], according to the Global Cancer Observatory (GLOBOCAN) 2024 data. Similarly, according to the Global Cancer Observatory (GLOBOCAN) 2024 data the incidence rate of breast cancer in Ethiopia is approximately 37.8 per 100,000 women [19] with mortality rate 21.4 per 100,000 women [21]. This high incidence makes it one of the most commonly occurring cancers worldwide. These statistics highlight the critical need for ongoing research, early detection, and effective treatments to manage and reduce the impact of breast cancer globally.

Despite being the second most common cancer overall cancers, breast cancer has a relatively low death rate. This lower mortality rate places it sixth in terms of cancer-related deaths, behind cancers such as liver cancer. The discrepancy between its high incidence and lower death rate can be attributed to advancements in early detection, established treatment improvements on traditional treatment modalities like radiotherapy [22-23], chemotherapy [24-27] and surgery [28] and recent developed treatment modalities like nanotechnology and immunotherapy, and better management strategies. These advancements collectively contribute to the improved survival rates and better management of breast cancer [29]. This focus on breast cancer allows for a deeper understanding of its dynamics and continued progress in reducing its burden on public health.

One of the advancement that improved cancer treatment modality was the invention of the laser trapping [LT] technology which was first discovered in the early 1980s [30–31] by Ashkin. The term ‘LASER’ is an acronym for Light Amplification by Stimulated Emission of Radiation. Light is generally accepted to be electromagnetic radiation and laser is an instrument that amplifying the light through radiation stimulation. Laser has many medical applications including treatment of cancer through laser therapy and laser trapping technology offers a powerful set of tools for cancer research and treatment by enabling precise manipulation and analysis of cancer cells and particles.

Another basic method used in enabling precise manipulation and analysis of cancer cells is attaching the cells with magnetic beads. Magnetic beads are small, spherical particles coated with various surface ligands that can be attracted to or repelled by magnetic fields. They are often used in conjunction with cell lines such as BT20 in various biological and biomedical

applications, including cell separation, enrichment, and analysis due to their ability to selectively isolate and manipulate cells or molecules [32-33].

Generally, the breast cancer cell lines used in this study to explore the electrical properties of the two hours treated 4T1 breast cancer cell lines that are treated by chemotherapy medication using an anticancer drug 2-Dodecyl-6-methoxycyclohexa-2, 5-diene-1, 4-dione (DMDD) that was obtained through multi-step extraction from the root of the star fruit plant Averrhoa carambola L., which is one of the Traditional Chinese Medicines (TCMs) [34-37]. Averrhoa carambola L. plant is the family of Oxalidaeae and native to Southeast Asia and was developed in Sri Lanka, India, and the Moluccas. Additionally, it is grown in French Polynesia, Guyana, Ghana, and Brazil. The plant looks like figure 1.1 below. Because of its chemical makeup, which includes the following: protein 0.38g, lipids 0.08g, carbs 9.38g, fiber 0.80-0.90g, water 80%, vitamins A, E, group B, and C, and minerals like Ca, Fe, Mn, Mg, P, Na, Zn, and high concentrations of K, it is utilized for a variety of purposes, including nutrition, medicine, and toxicology.

Figure 1.1 shows (a) Averrhoa carambola (star fruit) plant full description, (b) its leaves and flowers on parts of its branches.

On the other hand the BT20 breast cancer cell lines we used were those mixed with 3.1µm diameter polymer coated spherical magnetic beads in investigating the effect of magnetic beads on the ionization properties of BT20 breast cancer cells.

1.1. Objectives of the study

The objective of this study contains general and specific objectives.

1.1.1 General Objective:

To explore the electrical properties of pre-ionized 2h treated 4T1 breast cancer cells and examine the effect of magnetic beads on the ionization of BT20 breast cancer cells using optical tweezers.

1.1.2 Specific Objectives

1. To assess and measure the charges developed on 2h treated 4T1 breast cancer cells when they are trapped using optical tweezers.
2. To calculate the trap strength of optical tweezers by analyzing the forces applied to 4T1 cells within the laser trap.
3. To derive the Equation of Motion for Trapped 4T1 breast cancer cells as they are trapped and stabilized at the center of the optical trap.
4. To investigate how magnetic beads influence the ionization process of BT20 breast cancer cells and understands their interaction with the laser trapping system.

1.2 Brief description of the study

This study contains about five chapters. In chapter one, we introduced the cancer disease burden and used treatment modalities. In chapter two, we discussed about the general back ground of the study and literature reviews on breast cancer treatment modalities used different times. Chapter three contains about materials and methodology used to carried on this study. The results from measurements (experiments), calculations, and from fitting functions, with their analysis, were well discussed in chapter four. Finally in chapter five, we have drawn the conclusion from the results and discussions.

CHAPTER 2

2. General Background and Literature Review

2.1 General Background

In this section the overviews of the normal human cell, cancer cell, breast cancer, 4T1 and BT20 breast cancer lines, cell membrane, membrane transport, membrane potential, electromagnetic interaction, electrical properties of cells, electroporation, chemotherapy, magnetic beads and laser trapping technique are explained.

2.1.1 Normal human cell

Cells are the fundamental units of life in the living things, each performing specific functions that contribute to the overall health and operation of the living things. So for human, normal human cells are the basic structural and functional units of all tissues and organs in the human body. They are eukaryotic cells, which mean they contain a defined nucleus and various specialized organelles. These cells body develop, grow, and die in order to preserve homeostasis, a state of balanced health. The capacity to exchange information both inside and between other cells characterizes normal cells. One fundamental aspect is that the body's cells work together to coordinate information in order to integrate and regulate cellular processes, including growth. When the body is injured, normal cells multiply and either creates new cells or scar tissue to replace the damaged and killed ones. Normal cells grow in an ordinary manner, establish close bonds with their neighbors, and stop growing when they heal damage because of contact inhibition. Once there are sufficient cells, normal cells cease to divide. Since the DNA and RNA have regular functions, they carry characteristics that are necessary for those functions. Signals that determine whether a cell should divide, change into a different type of cell, or die are sent to these cells. They carry out a number of tasks, including supplying nutrients like vitamins, minerals, lipids, carbohydrates, and amino acids, and they also have a preset shape. They have a single nucleus, a nucleolus, and a vast cytoplasm [39-42].

2.1.2 Cancer cell

Cancer is a pathological condition characterized by the abnormal and uncontrolled proliferation of cells. It can develop virtually in any tissue or organ in the body and is marked by a series of disruptions in normal cellular processes. Cancer can be resulting in the formation of tumors and

the potential spread of these abnormal cells to other parts of the body (metastasis). This uncontrolled cell growth is the result of genetic mutations that drive the cells to bypass normal regulatory mechanisms governing cell division and tissue homeostasis [43]. Normal cells follow tightly regulated pathways that control cell division, differentiation, and death but in cancers, these regulatory mechanisms are disrupted and leading to the aberrant (uncontrolled) proliferation of cells which might resulted in insensitivity to growth inhibitors and evasion of apoptosis (programmed cell death) [43]. The formed tumors can be benign (non-cancerous) or malignant (cancerous). Malignant tumors have the ability to invade surrounding tissues and spread to other parts of the body through the blood or lymphatic system to establish secondary tumors in distant organs by metastasis. This makes complicate the treatment and management of the disease [44].

2.1.3 Breast cancer

Breast cancer is a multifaceted disease characterized by the uncontrolled growth of abnormal cells in breast tissue, often due to genetic mutations. Inherited mutations in the BRCA1 and BRCA2 genes notably heighten the risk of developing breast cancer by disrupting normal cell growth and apoptosis [43, 45]. Like other cancers, breast cancer involves tumor formation and metastasis. Environmental risk factors, including estrogen exposure, smoking, obesity, and alcohol consumption, also contribute to its development [46]. Breast cancer treatment typically includes surgery, chemotherapy, radiation, and hormone therapy, all of which can affect physical health and quality of life [47]. The disease also often leads to considerable emotional and psychological stress, such as anxiety and depression [48]. Additionally, the financial burden of diagnosis, treatment, and long-term care can be significant for both patients and healthcare systems [49].

Breast cancer cells are differ in terms of their biological environments, experimental outcomes, and the insights they provide, and can be grouped as in vivo and in vitro models breast cancer cell lines. In vitro models, studies are conducted in controlled environments outside of living organisms, typically in laboratory dishes or flasks. These studies use isolated cells or cell lines to investigate cellular behaviors, responses to treatments, and molecular mechanisms. This controlled environment offers precise experimental conditions, such as nutrient availability, temperature, and exposure to drugs or treatments that simplifies the system to focus on specific cellular or molecular processes without the complexity of whole organism interactions. Cell lines such as MCF-7 (estrogen receptor-positive human breast cancer cell line commonly used to study hormone-responsive breast cancer), MDA-MB-231 (triple-negative breast cancer cell line used to investigate aggressive cancer behavior and treatment resistance), and BT20 (human breast cancer cell line that is estrogen receptor-negative and used for studying breast cancer biology in a different hormonal context) can be grouped under this types [50].

In vivo models, studies involve experimenting with whole organisms or animal models. These studies evaluate how treatments affect cancer growth, metastasis, and overall physiology within the context of living system; provide a more accurate representation of how tumors interact with the host organism, including the immune system, blood supply, and tissue microenvironment, and offer insights into how treatments might perform in humans, addressing factors like drug metabolism, biodistribution, and systemic effects. Cell Lines such as 4T1 (murine breast cancer cell line used for studying breast cancer in animal models, especially for metastasis research), Xenograft model**s** human breast cancer cell lines like MCF-7 and MDA-MB-231 are implanted into immunocompromised mice to study tumor growth and response to therapies [51-52], are classified into these groups. In vitro and in vivo models serve complementary roles in breast cancer research. In vitro studies provide detailed insights into cellular and molecular mechanisms, while in vivo studies offer a broader understanding of how treatments perform in a whole organism. Both approaches are essential for developing and validating new therapies and improving our understanding of breast cancer biology.

2.1.4 4T1 and BT20 breast cancer cell lines

The 4T1 and BT20 cell lines are both commonly used in breast cancer research, but they have distinct origins and characteristics. 4T1 breast cancer cell line was derived from a spontaneous mammary tumor in a BALB/c mouse and it is a murine (mouse) breast cancer cell line [53]. This cell line is highly aggressive and metastatic, making it an excellent model for studying advanced breast cancer, tumor progression, and metastasis. It is particularly valuable for research on cancer-immune system interactions due to its ability to form tumors and spread to distant organs in mice [54]. On the other hand, BT20 cell line was derived from a human breast carcinoma and is one of the earliest established human breast cancer cell lines [55]. It is the cell line that is estrogen receptor-negative and has lower invasiveness. BT20 is utilized to investigate estrogen-independent pathways and the fundamental biology of breast cancer, as well as to evaluate the effects of various treatments on human breast cancer cells [55].

2.1.5 Cell membrane

The cell membrane, also known as the plasma membrane, is a crucial component of cells. It has only 5 to 10 nm in thickness and acts as a selective barrier, separating the internal environment of the cell from the external environment. It maintains the integrity of the cell and its internal components. It regulates the movement of ions, nutrients, and waste products through various mechanisms, including passive diffusion, facilitated diffusion, and active transport. The membrane contains receptors that bind signaling molecules (like hormones), enabling the cell to respond to external signals. It plays a role in cell recognition and adhesion through glycoproteins

and glycolipids, facilitating interactions with other cells and the extracellular matrix. The cell membrane is primarily composed of a phospholipid bilayer with embedded proteins, and often described by the fluid mosaic model [56] (as shown on figure 2.1 below). The phospholipid bilayer consists of two layers of phospholipids. Each phospholipid molecule has a hydrophilic (water-attracting, polar region) globular head and two hydrophobic (water-repelling, non-polar) fatty acid tails. The heads face outward towards the aqueous environment, while the tails face inward, away from water, creating a hydrophobic core. There are two types of proteins that are introduced into this bilayer: integral proteins and peripheral proteins. Integral proteins span the entire membrane and are involved in transport, acting as channels or carriers for molecules to pass through (example ion channels and glucose transporters). Peripheral Proteins are attached to the outer or inner surface of the membrane and play roles in signaling and maintaining the cell's shape. They are not embedded in the lipid bilayer but interact with the membrane or other membrane proteins. The cell membrane also contains components such as glycoproteins and glycolipids, carbohydrates and Cholesterol. Glycoproteins and glycolipids are carbohydrates attached to proteins (glycoproteins) or lipids (glycolipids) on the extracellular surface of the membrane. They play critical roles in cell-cell recognition and communication. Carbohydrates are often attached to proteins or lipids on the extracellular side of the membrane and contribute to the formation of the glycocalyx, which is involved in protection, immunity to infection, and regulation of cell growth. Cholesterol is interspersed within the phospholipid bilayer and its molecules help to stabilize the fluidity of the membrane, making it less permeable to very small water-soluble molecules.

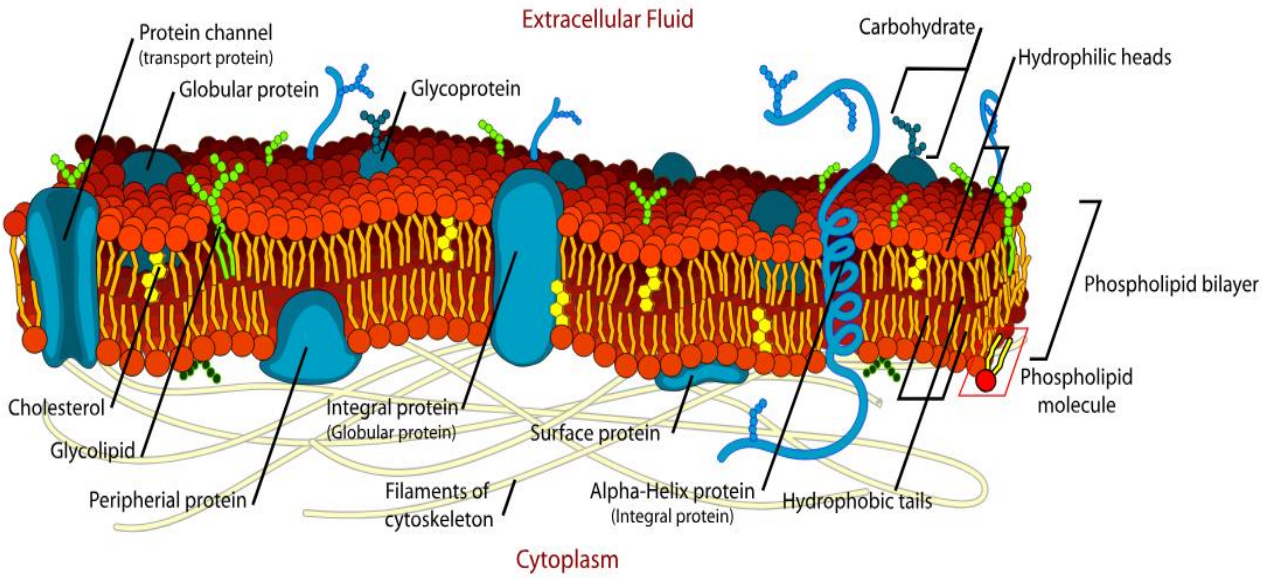

Figure 2.1 shows mosaic model of membrane structure and lipid bi-layer [56-59].

2.1.6 Membrane transport

Membrane transport is a fundamental process in cellular biology, allowing cells to exchange substances with their environment and maintain homeostasis. The membrane transport proteins are responsible to maintain homeostasis. These membrane transport proteins can be divided into two as: (1) ***Carrier proteins***: are bind to specific molecules and undergo conformational changes to transport these molecules across the membrane. Carrier proteins can be uniporters (transport one type of molecule), symporters (co-transport two types of molecules in the same direction), or antiporters (exchange one type of molecule for another in opposite directions). Examples of such proteins include glucose transporters that facilitate the uptake of glucose into cells, sodium-potassium pump which moves sodium out of the cell and potassium into the cell. Large molecules like sugar, carbohydrates, and amino acids are helped to travel from gradients of high concentration to gradients of low concentration. Diagram on figure 2.2 below illustrates its external and internal structure.

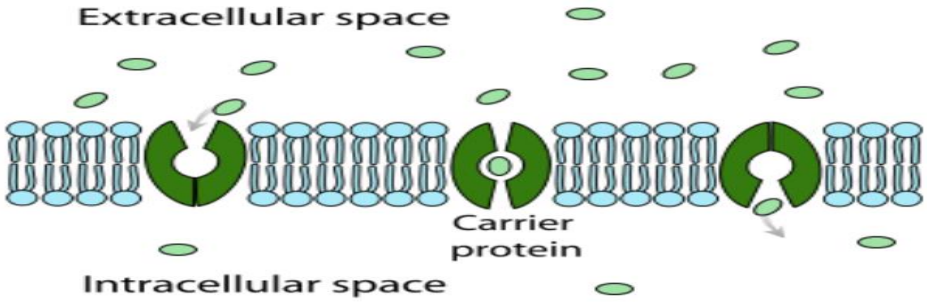

Figure 2.2 shows the structure of carrier protein [60].

(2) ***Channel proteins***: are the proteins which create tiny holes through which the membrane's permitted molecules of the right size can pass. They are employed in the transport of charged (ion such as Na^+, K^+, Cl^-) or polar (like water) molecules. Every molecule has a distinct channel protein; for instance, water diffuses across the plasma membrane via a protein channel known as an aquaporin. Rapid water passage across the membrane is made possible by aquaporin's, which are also crucial for red blood cells and specific kidney regions (where they reduce the quantity of water lost as urine). These channel proteins are further divided in two types as: Leak channels, which are continuously opened and Gated channels, which are stimulus (opening and closing in response to specific signals). Figure 2.3 below shows the structure of channel protein.

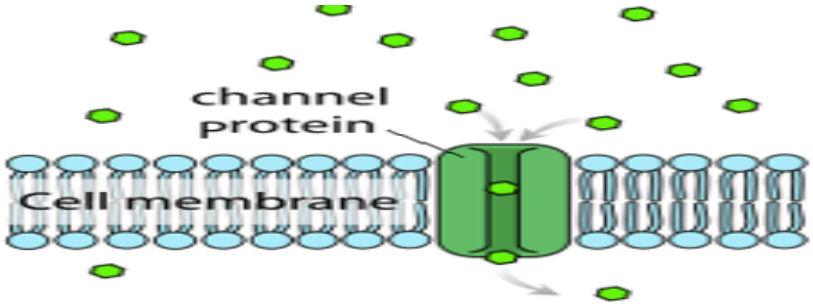

Figure 2.3 shows the structure of channel protein [60].

The membrane transport can be divided into two as passive and active transport. Passive transport is the movement of substances across the cell membrane without the use of cellular energy (ATP) and mostly facilitated by channel proteins. While some carrier proteins facilitate passive transport, others can perform active transport when they are connected to an ATP source [61]. Active transport, in which a molecule is transported against its concentration gradient to maintain concentration gradient across the membrane which helps to balance the osmotic pressure on either side of the membrane [62], uses metabolic energy to transport molecule across the membrane. The interior plasma membrane is negatively charged relative to exterior part of the cell and this determines the movement of charged particles. Example Potassium ion (K^+) attracts Cl^- and forces out of the cell by the negatively charged interior part of the membrane [63]. The membrane permeability to a substance depends on the molecule's size, lipid solubility, and electrical charge. Gases such as oxygen (O_2), carbon dioxide (CO_2), and nitrogen (N_2), hydrophobic molecules such as steroid hormones, and weak organic acids and bases readily diffuse through the cell membrane. Water and urea are examples of small, uncharged polar molecules that can permeate the lipid bi-layer. Large or small charged particles (like amino acids) or ions (like Na^+, K^+, Cl^-, and Ca^{2+}) cannot permeate through the lipid bi-layer. Instead, they pass through specialized membrane channels as they facilitate and often allowing significant quantities to move in and out of the cell [64].

2.1.7 Membrane Potential

Membrane potential, also known as trans-membrane potential, is the difference in electric potential between the interior and the exterior of a cell membrane. It arises due to the differential distribution of ions across the cell membrane [65]. In other words, the system of ion pumps and channels causes the cell plasma membrane to experience resting trans-membrane voltage, or electric potential difference, under normal physiological conditions when it is not exposed to an external electric field [66]. For a cell at rest, the balance between the diffusion and electric force leads to unbalance in electrical between the intracellular and extracellular membrane. This leads

the membrane in a potential difference which is known as membrane potential. This potential is typically between -35mV and -90mV [67], with the negative sign indicates that the inside of the cell is more negatively charged compared to the outside. This negative charge resulted from a higher activity of chloride (negative) ion pumps relative to sodium or calcium (positive) ion pumps [68].

When the membrane potential becomes less negative, the cell is depolarized, and when it becomes more negative, the cell is hyperpolarized [67]. Changes in membrane potential, caused by fluctuations in ion concentrations and surface charge, activate voltage-gated ion channels [69]. This leads to variations in intracellular ion concentrations, generating action potentials and influencing signaling pathways [70]. For example, fluctuations in Ca^{2+} levels can impact crucial cellular processes such as migration, proliferation, attachment, necrosis, and apoptosis [71].

2.1.8 Electrical properties of cells

Electrical properties of cells encompass the cell membrane's ability to conduct and respond to electrical signals, including membrane potential, ionic currents, ion channel activity, electrical resistance, and capacitance [72] and the major part of electrical properties in cells are dependent on cell membranes and its composition [73]. Electrical properties like membrane potential are fundamental for generating and transmitting action potentials, which are essential for cellular communication and physiological responses [65]. The electrical properties of cells regulate the movement of ions across the membrane through channels and pumps, maintaining homeostasis and controlling cellular activities such as muscle contraction and neurotransmitter release [72]. Proper ion regulation and membrane potential maintenance are vital for cell survival and function. Disruptions can lead to diseases, including cancer and cardiovascular conditions [72]. These properties are critical for understanding how cancer cells deviate from normal cells and contribute to their malignancy.

Normal cells typically have a resting membrane potential (RMP) around -60 to -70 mV, maintained by the Na^+/K^+ ATPase pump, which balances the ion gradients across the cell membrane and it is influenced by the K^+, Na^+, and Cl^- gradients, with K^+ being more permeable at rest, contributing to the negative internal potential. Cancer cells often exhibit a more depolarized membrane potential, which can be around -30 to -50 mV, due to altered ion channel expression and activity. This depolarization can affect cellular signaling and proliferation [74]. Cancer cells frequently show altered ion gradients and channel activities, including increased Na^+ influx and K^+ efflux, which can contribute to their malignant behavior [75]. Normal cells have a balanced expression of voltage-gated and ligand-gated ion channels, which regulate cellular excitability and signal transduction whereas cancer cells often express different types or

quantities of ion channels compared to normal cells. For instance, they may have up regulated expression of voltage-gated Na^+ channels or down regulated K^+ channels [75]. Channels such as K^+ play crucial roles in maintaining the RMP and regulating cellular responses to external stimuli in normal cells [76], but abnormal channel function can lead to altered cell proliferation, migration, and apoptosis, contributing to the aggressive nature of cancer [77].

Normal cells generally have a characteristic electrical resistance related to their membrane composition and ion channel activity while cancer cells often exhibit decreased electrical resistance due to increased ion channel activity and changes in membrane properties [78]. The capacitance of the cell membrane, related to its lipid bilayer, is typically around 1 $\mu F/cm^2$, reflecting its ability to store and separate electrical charges and cancer cells can show altered membrane capacitance, which may be linked to changes in membrane composition or surface area [79].

2.1.9 Electromagnetic interaction

Electromagnetic (EM) interaction refers to the forces between charged particles due to their electric and magnetic fields. In the context of cells, it involves interactions between ions, molecules, and cell membranes influenced by electric and magnetic fields. Maxwell equations can be used to model the propagation of light through biological tissues, how light diffuses through tissues, help to describe how light waves are affected by the tissue's permittivity and permeability (which influence how light is absorbed, scattered, and transmitted), how it interact with matter and are central to understand electromagnetic wave behavior in any medium [80]. The permittivity of cellular components, like the membrane and cytoplasm, influences the speed and attenuation of light as it passes through the cell, reflects off (high permittivity lead to greater reflection.), scatters(sensitive to changes in the refractive index) or absorbs (high permittivity regions can absorb more light) [81]. Techniques like optical coherence tomography (OCT) or fluorescence microscopy rely on differences in permittivity between cellular structures and the surrounding medium to produce contrast in images. Polarization also provides additional contrast and information through changes in how light is reflected, scattered, and emitted, revealing structural and molecular details [82-83]. Additionally, magnetic beads modify light interactions through their scattering, absorption, and fluorescence properties, enhancing imaging and analysis capabilities. As a whole, these effects enable advanced imaging, analysis, and manipulation of cells, providing valuable insights into cellular functions, molecular interactions, and structural characteristics [84-87].

2.1.10 Electroporation

Electroporation is a technique used to introduce molecules, such as DNA, RNA, or drugs, into cells by applying an electric field to temporarily increase the permeability of the cell membrane [88]. Cells are typically suspended in a conductive solution or placed in a specific electroporation buffer that ensures effective transmission of the electric field and can help protect the cells during the process. A brief, high-voltage electric pulse is applied to the cells and it generates an electrostatic force that temporarily disrupts the lipid bilayer of the cell membrane, forming pores (causes the cell membrane to become permeable) [89], which allowing the introduction of exogenous molecules into the cell. After the electric pulse, the cell membrane begins to reseal, and the pores close. Cells are then allowed to recover and express or utilize the introduced substances [90]. The cells are typically incubated in a recovery medium to facilitate the reestablishment of normal cellular functions and membrane integrity.

Electroporation is widely used to introduce genetic material into cells, such as plasmids for gene expression studies, gene therapy, or the creation of genetically modified organisms [88], to deliver therapeutic drugs into cells, which enhance the effectiveness of drug delivery systems especially for cell treatments [89] and to improve the delivery and efficacy chemotherapeutic agents [91].

2.1.11 Chemotherapy

Chemotherapy is a type of cancer treatment that uses chemical substances, usually cytotoxic drugs, to kill or inhibit the growth of cancer cells. The process begins with the diagnosis of cancer and the determination of the appropriate chemotherapy regimen based on the type, stage, and genetic characteristics of the cancer [92]. The drugs can be administered orally (by mouth), intravenously (through a vein), or through other routes depending on the specific drug and treatment plan [93] and usually given in cycles [92].

Chemotherapy can be used for cancer cell destruction [93], tumor shrinkage (often used to shrink tumors before surgery, neo-adjuvant therapy or to eliminate any remaining cancer cells after surgery, adjuvant therapy) [92] or metastasis control [92]. Chemotherapy is a cornerstone in the treatment of various cancers, providing an option to treat cancers that are not amenable to surgery or radiation alone [94], has significantly contributed to the increased survival rates for many types of cancer [92] and is often used in combination with other treatments [93].

2.1.11 Magnetic beads

Magnetic beads are small, spherical particles that made from materials that can be magnetized, such as iron oxide and operate based on their magnetic properties. They are typically in the range of nanometers to micrometers in size and can be manipulated using external magnetic fields. Their surface is coated with specific molecules, such as antibodies, which can bind to target substances (example, coated with antibodies that specifically bind to cancer cells). They can be used to deliver chemotherapy drugs directly to target cells, separate specific types of cells from mixture, facilitate the sorting of specific cell types, study biomolecular interactions, including protein-protein interactions and DNA-protein interactions and they can help in studying the efficacy of chemotherapy drugs by enabling targeted drug delivery, analyzing drug-cell interactions, and assessing cellular responses to treatments [95].

There are different types of magnetic beads suitable for near infrared (NIR) laser irradiation of breast cancer cells. The choice of magnetic beads depends on their material, functionalization, and magnetic properties. Magnetic beads such as polymers, iron oxide (Fe3O4), gold-coated magnetic beads, core-shell magnetic nanoparticles, and magnetic beads with photothermal agents are some types with specific properties and functionalizations for NIR laser irradiation of breast cancer cells. Iron oxide (Fe3O4) magnetic beads are composed of magnetic iron oxide nanoparticles, which can be easily manipulated using external magnetic fields. They are often used for imaging and therapeutic applications due to their biocompatibility and magnetic properties. They can be coated with various ligands or antibodies to target specific cancer cell markers, and combined with NIR-sensitive materials to enhance local heating and improve the efficacy of photothermal therapy [96]. Gold-coated magnetic beads are combine magnetic cores with a gold shell. The gold shell provides additional functionality, such as enhanced optical properties and the ability to absorb NIR light for photothermal effects. They can be modified with targeting agents, such as antibodies or peptides, to specifically bind to breast cancer cells, and the gold shell allows for efficient NIR light absorption, which can be used to generate heat for localized destruction of cancer cells [97]. Core-shell magnetic nanoparticles consist of a magnetic core (e.g., iron oxide) and a shell made from various materials, including silica or polymers. The shell can be engineered to provide stability, biocompatibility, or additional functionalization, can be tailored with targeting molecules and imaging agents, and chosen to optimize NIR light absorption and photothermal effect, enhancing the therapeutic efficacy of laser treatments [98]. Magnetic beads with photothermal agents incorporate photothermal agents such as dyes or nanomaterials that absorb NIR light and convert it to heat. The magnetic component allows for targeted delivery and manipulation of the cancer cells. The embedded photothermal agents enhance the localized heating effect upon NIR irradiation, improving the efficacy of thermal therapy.

2.1.12 Laser Trapping Technique

Laser trapping, also known as optical trapping or optical tweezers, is a technique that works using the principle which relies on the interaction between light and matter, utilizes the radiation pressure of a focused laser beam to trap. Laser beam focused through a microscope objective lens, creates a highly intense spot of light and generates an optical gradient force that is responsible for trapping particles or cells (e.g., cancer cells) [99].

The forces involved in optical trapping are critical for understanding how laser tweezers can hold and manipulate particles. These forces are the gradient of the laser beam (which pulls the particles towards the focal point) and the scattering force (which pushes them away from the beam). The gradient force arises from the spatial variation in the intensity of the laser beam. In a focused laser beam, the intensity of light is highest at the center (the focal point) and particles that are placed in this high-intensity region experience a force directed towards the focal point due to the differential absorption and scattering of light [100]. Mathematically it can be described by the equation, $F_{\text{grad}} = \frac{1}{2}\alpha\nabla I$ 2.1

where α is the polarizability of the particle which is a measure of how easily the particle electron cloud can be distorted by external electric field such as that of a laser beam, depends on the particles material properties, shapes and sizes. For dielectric particles, the polarizability is related to the particle volume and its relative refractive index compared to the surrounding medium. And ∇I is the gradient of the light intensity refers to how the intensity of the laser beam changes with position. In a focused laser beam, intensity is highest at the focal point and decreases as you move away from this point. The gradient represents the rate of change of intensity in space, which creates a force that pulls particles toward regions of higher intensity. In laser trapping, particularly in optical trapping or optical tweezers, the commonly used beam intensity distribution is the Gaussian beam profile, which has a bell-shaped intensity distribution where the intensity is highest at the center of the beam and decreases towards the edges. This distribution is ideal for trapping particles because it creates a gradient of light intensity that generates the gradient force [101]. So, for Gaussian intensity distribution intensity as a function of distance from beam center (r) can be given as, $I(r) = I_0 e^{-\frac{r^2}{b^2}}$, where I_0 the peak value of intensity and b is the waist radius of intensity (radius at which I falls to $\frac{1}{e^2}$ of I_0). Then the gradient of intensity over distance r is, $\nabla I(r) = -\frac{2rI_0}{b^2} e^{-\frac{r^2}{b^2}}$ and finally the gradient force, F_{grad} becomes, $F_{\text{grad}} = \frac{1}{2}\alpha\nabla I = --\frac{rI_0\alpha}{b^2} e^{-\frac{r^2}{b^2}}$ 2.2

The scattering force arises from the momentum transfer of photons that are scattered by the particle. When a particle is not perfectly aligned with the optical axis, photons striking the particle scatter in different directions, imparting a force that pushes the particle away from the center of the beam [102]. When a particle is not perfectly aligned with the optical axis of the beam, photons scatter in various directions. The momentum transfer from the scattered photons results in a net force on the particle. The power of the laser beam determines the number of photons interacting with the particle and hence the scattering force. When using NIR lasers to trap breast cancer cells, the Mie scattering regime is typically applicable because the breast cancer cells are generally much larger than the wavelength of NIR light [103].

The effective trapping of particles occurs when the gradient force is strong enough to counteract the scattering force. The balance between these forces ensures that particles can be stably trapped and manipulated within the focal volume of the laser beam. By adjusting parameters such as laser power, wavelength, and the numerical aperture of the objective lens, researchers can fine-tune the balance between gradient and scattering forces. Higher laser power increases both forces, but the gradient force increases more sharply, leading to stronger trapping.

Laser trapping is a powerful technique used in various scientific fields and modern optical trapping systems use sophisticated feedback mechanisms and dynamic adjustments to control and measure forces at the pico-Newton scale, enabling precise manipulation of particles and molecules for purposes such as cell sorting, cell interactions, force measurements (the forces exerted by cells, such as the forces generated during cell-cell interactions), biophysical measurements (the mechanical properties of biological samples like elasticity or stiffness and viscosity)[104-105].

In combination with electroporation, laser trapping can position cells or magnetic beads precisely, ensuring targeted application of the electric field, improving the accuracy and reproducibility of electroporation experiments [99]. This novel method is entirely a new technique that has different applications in experimental physics, biophysics, experimental statistical physics and nanotechnology due to their ability of precisely manipulation.

2.2 Literature Review

Magnetic beads, Chemotherapy and NIR Laser Irradiation in Cancer Cells Therapies

In this section the effects of near infrared (NIR) laser irradiation alone, NIR laser irradiation combined with chemotherapy, NIR laser irradiation combined with magnetic beads, and NIR

laser irradiation combined with both magnetic beads and chemotherapy on cancer cell as explored by different studies were explained, especially by focusing on 4T1 and BT20 breast cancer cell lines and others.

2.2.1 NIR Laser Irradiation Alone in Cancer Cells Therapies

NIR laser irradiation is a promising technique for the study and treatment of breast cancer cells. Studies involving how specific breast cancer cell lines such as 4T1, BT20, and other response to NIR laser irradiation have demonstrated in various applications including photothermal therapy, photodynamic therapy, and imaging. In photothermal therapy (PTT), the effectiveness of gold nanorods (GNRs) for targeted therapy in 4T1 cells was investigated. They experienced significant thermal damage and cell death when treated with GNRs and irradiated NIR lasers. The uses of GNRs allowed for precise targeting and effective destruction of cancer cells, with minimal effects on surrounding tissues [106]. In BT20 cell lines the use of silica-coated gold nanoparticles for PTT is explored and the results demonstrated that NIR laser irradiation effectively heated the nanoparticles, leading to substantial cytotoxic effects [107].

In photodynamic therapy (PDT), the upconversion nanoparticles (UCNPs) that are responsive to NIR light in 4T1 cells are used and the NIR laser irradiation of UCNPs generated reactive oxygen species (ROS) that induced cell death. This approach demonstrated improved therapeutic efficacy with deeper tissue penetration due to the NIR light and efficient ROS generation [108]. Again in BT20 cells the use of porphyrin-loaded nanoparticles activated by NIR light is investigated and NIR irradiation triggered the photosensitizer, leading to significant ROS production and effective killing of cells [109].

In imaging applications, the study utilized that NIR fluorescence imaging with quantum dots (QDs) are used to visualize 4T1 cells and demonstrated as the NIR fluorescence provided high-resolution images of the cells, aiding in monitoring and diagnosing breast cancer. The targeted QDs allowed for enhanced imaging contrast and specificity [110]. In case of BT20 cells, the multimodal NIR imaging and therapy using conjugated polymer nanoparticles (CPNPs) are explored and the NPs enabled both imaging and therapeutic applications, providing detailed information on cellular responses to NIR laser irradiation and effective treatment through combined imaging and therapy [111].

In comparing the effects of NIR laser-induced PTT and PDT across other breast cancer cell lines, such as MCF-7, and MDA-MB-231, PTT is generally effective across all cell lines and PDT showed variability depending on the cell line's uptake of photosensitizers and inherent cellular properties. 4T1 cells and BT20 cells exhibited robust responses to both therapies, while other

lines showed more mixed results [112]. MCF-7 cells, which are estrogen receptor-positive and generally less aggressive, show more variability in response to PDT and their effectiveness can vary based on factors such as the type and concentration of photosensitizers used, as well as their intrinsic cellular properties which may affect the generation and handling of ROS [113]. MDA-MB-231 cells**,** triple-negative breast cancer cells, have mixed responses to PDT. While they uptake photosensitizers well, their aggressive nature and ability to repair oxidative damage can sometimes mitigate the effectiveness of PDT. Thus, optimizing PDT conditions for this cell line is crucial for achieving consistent therapeutic outcomes [114].

2.2.2 NIR laser irradiation combined with magnetic beads

Combining magnetic beads with NIR laser irradiation represents a novel and versatile approach in the treatment and study of breast cancer cells that leverages the unique properties of magnetic beads for targeted therapy and NIR laser for activation and imaging. In photothermal therapy it was showed that, when magnetic beads were functionalized with anticancer to specifically target 4T1 cells and exposure to NIR laser, the beads generated localized heat, resulting in significant thermal damage to the cells. In this approach, high specificity and reduced off-target effects was demonstrated [115]. In BT-20 cells it also reported that, when magnetic beads loaded with a chemotherapeutic agent were used to target the cells and NIR laser irradiation was applied to activate the drug, a significant reduction was observed. Here, magnetic beads provided targeted delivery of the drug, while NIR laser irradiation increased the overall effectiveness of the treatment [116]. The effectiveness of magnetic bead-assisted NIR photothermal therapy in breast cancer cell lines, such as MCF-7, MDA-MB-231, 4T1 and BT20, varied due to variations in magnetic bead uptake and cellular responses to thermal damage. The 4T1and BT20 cell lines showed higher sensitivity to photothermal effects compared to MCF-7 and MDA-MB-231 [117].

In photodynamic therapy again, it has shown that magnetic beads combined with NIR laser irradiation significantly enhance the effectiveness of PDT in 4T1 cells by in concentrating the photosensitizers at the tumor site which improve the PDT outcomes (therapeutic efficacy, reduce side effects, and provide better control over tumor growth) by increasing ROS production [118]. In BT20 cells, magnetic bead-assisted PDT has shown promising results, the enhanced delivery of photosensitizers and increased light absorption due to magnetic beads, improve the PDT effectiveness that finally leads to better cellular damage and apoptosis compared to conventional PDT methods [119]. For MCF-7 cells, magnetic bead-assisted PDT has shown variable results. While magnetic beads improve the targeted delivery and activation of photosensitizers, the inherent lower aggressiveness and different cellular responses can affect the overall PDT effectiveness and the optimization of PDT parameters and bead properties are crucial for enhancing results in this cell line [120]. In MDA-MB-231 cells, magnetic bead-mediated PDT has demonstrated mixed results due to aggressive nature of these cells and their ability to repair

ROS-induced damage. Nevertheless, the enhanced delivery and activation of photosensitizers has shown potential for improving PDT outcomes with further optimization [121].

2.2.3 NIR laser irradiation combined with chemotherapy

Combining chemotherapy with NIR laser irradiation is another advanced approach in breast cancer treatment, can potentially improve treatment outcomes by addressing cancer cells from multiple angles, utilizes the synergistic effects of chemotherapy and involves a multifaceted approach that leverages the strengths of both modalities. NIR irradiation can enhance the cytotoxic effects of chemotherapy drugs through photothermal or photodynamic mechanisms and it can increase the permeability (tumor vasculature) of cancer cell membranes or tumors, facilitating better drug uptake and distribution.

In photothermal combined with chemotherapy, it was investigated that as the magnetic nanoparticles loaded (in vitro) or gold nanorods loaded (in vivo) with a chemotherapeutic agent were targeted to 4T1 cells and irradiated with NIR laser, the localized temperature increased and enhancing the release of the chemotherapy drug, improving its efficacy. This combined approach led to reduced tumor growth and increased survival rates in the 4T1 mouse model [122]. Another study on BT20 cells demonstrated that NIR laser irradiation significantly enhanced the cytotoxic effects of doxorubicin, led to greater cell death and reduced drug resistance compared to doxorubicin treatment alone and improved therapeutic outcomes by increasing the release of doxorubicin from the nanocarriers and induced additional thermal damage to the cells [123]. Across the various breast cancer cell lines, including MCF-7, MDA-MB-231, 4T1, and BT20, the studies evaluated efficacy of the combination therapy when different chemotherapy agents (e.g., doxorubicin, paclitaxel) were used with NIR laser irradiation and in all cell lines the improved treatment efficacy was observed. However, the degree of enhancement varied among cell lines, with 4T1 and BT20 cells showing the most significant improvements due to their higher sensitivity to photothermal effects, but MCF-7 and MDA-MB-231 cells benefited with a lesser extent [124]. Similarly, in photodynamic therapy combined with chemotherapy, NIR laser can activate photosensitizers that, when combined with chemotherapy, produce reactive oxygen species (ROS) to kill cancer cells, leading to improved treatment efficacy.

2.2.4 NIR laser irradiation combined with both magnetic beads and chemotherapy

Combining magnetic beads, chemotherapy, and NIR laser irradiation as single modality and using it, is a multifaceted approach for cancer treatment, aiming to enhance therapeutic efficacy and reduce side effects. This integrated strategy leverages the strengths of each modality, magnetic targeting, chemotherapeutic agents, and photothermal or photodynamic effects, to

achieve improved outcomes. The combined approach uses magnetic beads to deliver chemotherapeutic agents and/or photosensitizers, followed by NIR laser irradiation to activate the photosensitizers or photothermal agents. As an example, temperature-sensitive liposomes loaded with doxorubicin (DOX) and IR-780 have been shown to release drugs in response to NIR laser activation, leading to improved therapeutic outcomes [125]. Studies have reported the effects and uses of this more improved and effective treatment modality both in vitro and in vivo breast cancer cell lines.

In vetro studies, it was reported that the doxorubicin-loaded magnetic beads targeted to 4T1 cells combined with NIR laser irradiation led to a significant increase in cell death compared to doxorubicin alone [126], and Wang, H., investigated the magnetic bead-mediated paclitaxel delivery targeted to BT20 cells and subjected to NIR laser irradiation that resulted in significant cell death and improved therapeutic outcomes [127]. Again the effectiveness of magnetic bead-based drug delivery combined with NIR laser therapy across different breast cancer cell lines such as MCF-7 and MDA-MB-231 shown less improvement compared to 4T1 and BT20 cells explained by Chen, Y., [128].

Similarly in vivo studies, the therapeutic efficacy of doxorubicin-loaded magnetic beads combined with NIR laser photothermal therapy in a 4T1 murine model assessed and significant tumor regression and prolonged survival was reported by Kim, C., [129], and the effectiveness of magnetic bead-mediated paclitaxel delivery combined with NIR laser photothermal therapy in BT20 xenograft models tumor volume and therapeutic response were assessed and size reduction and improved therapeutic outcomes is resulted [130]. Similar to in vitro, other cell lines have shown lower significant improvements in treatment outcomes under magnetic bead-assisted chemotherapy combined with NIR laser therapy [131].

In summary, combining magnetic beads, chemotherapy, and NIR laser irradiation provides a sophisticated treatment approach by integrating targeted drug delivery, localized heating or activation, and enhanced therapeutic effects. This section highlights the effectiveness of this combined therapy in improving drug delivery, increasing therapeutic efficacy, and reducing side effects compared to traditional treatments and single treatment modality alone.

In this study in exploring the electrical properties of pre-ionized 2h treated 4T1 breast cancer cells, we used the combination of chemotherapy and NIR laser irradiation modality, with an anticancer compound 2-Dodecyl-6-methoxycyclohexa-2, 5-diene-1, 4-dione (DMDD) as medication drug and an infrared diode-pumped Nd:YVO4 laser, which lasing at a wavelength of 1064 nm. The compound DMDD was chosen due to, its chemical and pharmacological properties, its mechanism of action and its overall efficacy of treatment when combined with

laser trapping. DMDD is a synthetic compound that has cyclohexadienone derivative with a dodecyl chain and a methoxy group, which may influence its lipophilicity and interaction with biological membranes. DMDD has shown potential as an anticancer agent and its effectiveness can be attributed to its ability to interfere with cellular processes, potentially inducing apoptosis or disrupting cancer cell metabolism. DMDD might induce oxidative stress by generating reactive oxygen species (ROS), which can lead to cellular damage and apoptosis, particularly in cancer cells. The infrared diode-pumped Nd:YVO4 laser also chosen due to its high power, good beam quality, and efficiency. The 1064 nm wavelength is effective for various biological applications due to its deep tissue penetration, it can induce localized heating and photothermal effects in tissues which is useful for targeted therapy where the laser can selectively heat and destroy cancer cells. So, the combination of DMDD with the Nd:YVO4 laser can enhance the overall efficacy of treatment.

While in explaining the effect of magnetic beads attachment on the ionization properties of the untreated BT20 breast cancer cells, we used the combination of magnetic beads and NIR laser irradiation modality. We used an infrared diode-pumped Nd:YVO4 laser for irradiation and 3.1µm diameter polymer coated spherical magnetic beads. 3.1µm diameter polymer-coated spherical magnetic beads are specialized tools used in various biological and biomedical applications, including the study of cancer cells such as BT20 breast cancer cells. The types of 3.1µm diameter polymer-coated spherical magnetic beads widely used for these various applications include super-paramagnetic beads**,** magnetite (Fe_3O_4) beads and maghemite (γ-Fe_2O_3) beads.

Super-paramagnetic beads exhibit magnetic properties only in the presence of an external magnetic field and they lose their magnetism when it removed, which prevents clumping. These beads are widely used for cell separation and isolation due to their high responsiveness to magnetic fields. Magnetite (Fe_3O_4) beads are commonly used in biomedical applications and known for their high magnetic susceptibility and stability. They can be easily manipulated using magnetic fields and are often coated with various polymers for enhanced functionality.

Maghemite (γ-Fe_2O_3) beads are another type of iron oxide magnetic bead used in biomedical applications. They have similar properties to magnetite but with slightly different magnetic characteristics. These beads are chosen for their magnetic properties, size and biocompatiblities. The 3.1 µm diameter is suitable for cellular applications, allows the beads to interact effectively with cells without causing significant interference in cellular processes or being too large to pass through cellular membrane. These beads are designed to respond quickly and efficiently to magnetic fields, allowing for precise manipulation, separation, or sorting of cells and other biological particles. The polymer coatings often ensure that the beads are biocompatible, reducing potential toxicity or immune responses when used in biological systems. The polymer

coating on these beads can be customized to enhance their compatibility with biological systems. Common coatings include Carboxylate groups (useful for conjugating with proteins or antibodies), Polyethylene glycol (PEG, reduces nonspecific binding and increases biocompatibility) and Amino groups (useful for further functionalization or conjugation with various biomolecules). These magnetic beads generally allow for precise control over the interaction between BT20 cells and other substances, such as drugs or antibodies, facilitating studies on cell behavior, drug responses, or cellular mechanisms.

CHAPTER 3

3. Materials and Methodology

This chapter covered the culturing and treatment of 4T1 breast cancer cells, as well as the culturing of BT20 breast cancer cells and their subsequent mixing with magnetic beads. We also discussed the experimental setups, materials used, the mechanism behind membrane breakdown, and the operation of the trapping system.

3.1 4T1 and BT20 breast cancer cells culture

The samples of both 4T1 and BT20 cells were cultured at the International Ginseng Institute, Tennessee Center for Botanical Medicine Research, while the laser trapping experiments were conducted in the Department of Physics and Astronomy at Middle Tennessee State University. 4T1 cancer cells were cultured in RPMI1640 medium supplemented with 10% fetal bovine serum (FBS) in a 5% CO_2 and 37°C incubator. The cells were trypsinized (using trypsin to dissociate the cells from their culture vessel). The cells were passaged to fresh growth medium every 2-3 days. After trypsinization, the 4T1 cells were diluted in RPMI-1640 medium and seeded into a 96-well plate at a density of 5,000-7,000 cells per well (100 µL/well). Subsequently, the culture medium from each well was transferred to an Eppendorf tube. The wells were rinsed with FBS, and then 50 µL of trypsin was added to each well to detach the cells, which were then collected in the same Eppendorf tube [134-137].

The 4T1 breast cancer cells were treated with DMDD at a concentration of 100 µmol per well for two hours following a 24-hour attachment period to the well bottom. Each treatment condition included six replicate wells. While the BT20 breast cancer cells were mixed with 3.1µm diameter polymer coated spherical magnetic beads.

3.2 Experimental setup and Materials

The experimental design used in this study looks like the figure 3.1 below.

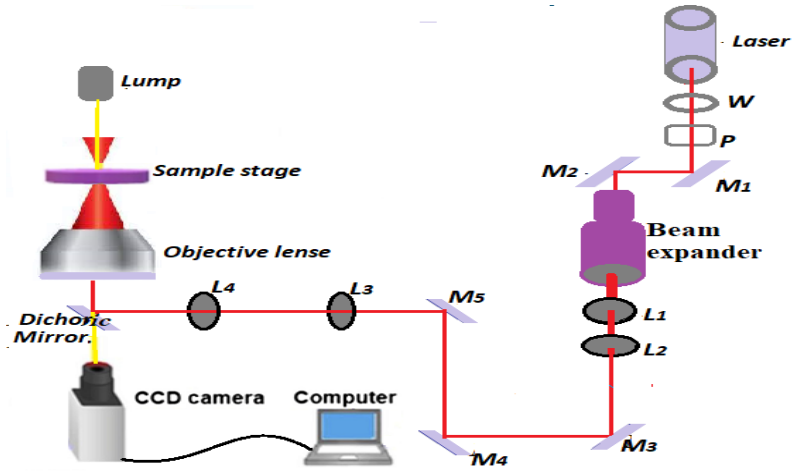

Figure 3.1 Experimental designs for the infrared laser trap.

An infrared diode-pumped Nd:YVO_4 laser, which operates at a wavelength of 1064 nm was used. This laser, using neodymium-doped yttrium orthovanadate as the gain medium, produces a highly focused and linearly polarized beam. The laser has a maximum output power of 8W and emits a beam with a diameter of 4 mm. To adjust the intensity of the laser beam, a polarizer (P) was employed. The laser beam is initially directed by mirrors M_1 and M_2 before passing through a 20× beam expander. This beam expander enlarges the beam's diameter, which is essential for the subsequent optical setup. The expanded beam then travels through a series of lenses to further manipulate its size and focus. Specifically, two lenses with focal lengths of 5 cm (L_1) and 20 cm (L_2) are used. The purpose of these lenses is to increase the beam's diameter to approximately 2 cm, which matches the diameter of the microscope's objective lens window. This expansion is crucial because it enhances the optical trap's strength. To optimize the beam's path and alignment, mirrors M_3 and M_4 are employed. These mirrors ensure that the beam is properly redirected and aligned. Mirror M_5 is strategically placed to create a steerable optical trap. It is positioned 20 cm away from converging lens L_3, which is itself positioned 20 cm away from another converging lens, L_4 that placed 20 cm away from the back of the objective lens. Both lenses L_3 and L_4 have the same focal length of 20 cm, and they are separated by a distance equal to twice their focal length (i.e., 40 cm). This setup fulfills the conditions of geometrical optics required to form a steerable trap precisely at the focal plane of the microscope. Once the beam is properly collimated and aligned, it is introduced into the microscope using a dichroic mirror (DM) positioned at a 45° angle within the microscope. The dichroic mirror has a dual function: it reflects the laser beam, directing it to the microscope 100× objective lens with a 1.25 numerical aperture for focusing, while simultaneously allowing the imaging light from an Olympus Tl4 halogen lamp to pass through. The transmitted imaging light is captured by a digital camera connected to the microscope via its second port, which is controlled by a PC. This setup enables simultaneous imaging and manipulation of samples under the microscope.

3.3 Working principle of the laser trap

When bead is trapped using a NIR laser, laser beam is precisely focused to a small spot, often at the focal plane of the microscope objective lens. The presence or absence of the bead affects the convergence the rays of light passing through the objective lens. When no present in the trap, the rays of light passing through the objective lens converge at the position of the laser true focus. As the bead inserted in to the trap and laser interacts with it, the position at which the rays of light passing through the objective lens converge (focus point) changes. When the bead is laterally centered in the beam focus, the forces due to the gradient of the beam intensity cancel out because the intensity gradient on either side of the bead is symmetrical, resulting in no net force pushing the bead to the left or right (as example see F_1 and F_2 on figure 3.2A). Even though the bead is centered and experiences no lateral force, an unfocused (diverging) laser beam can still cause a force (scattering force) due to the nature of the light propagation but the net force acts along the axial direction of the trap counteracts it. So, the balance between this axial gradient force and the scattering force results in the bead being stably trapped slightly downstream of the beam waist (see figure 3.2A below). When a bead is displaced to one side laterally or axially, the light rays passing near or through it are refracted, and the momentum can be transferred from the higher intensity and lower intensity region rays are different. This difference in momentum transfer causes a net force to be exerted on the bead. Specifically, the greater momentum changes from the more intense rays on one side of the bead results in a net force that pushes the bead back towards the center of the beam where the intensity is highest and the forces on the bead are more balanced (see figure 3.2B as example). In addition to centering the bead within the laser, a focused laser also maintains the bead in a stable axial position. The momentum change of the focused rays generates a force that pulls the bead towards the laser focus, whether the bead is positioned in front of (figure 3.2C) or behind the focus (figure 3.2D). Consequently, the bead will stabilize slightly behind the focus, where this force counteracts the scattering force.

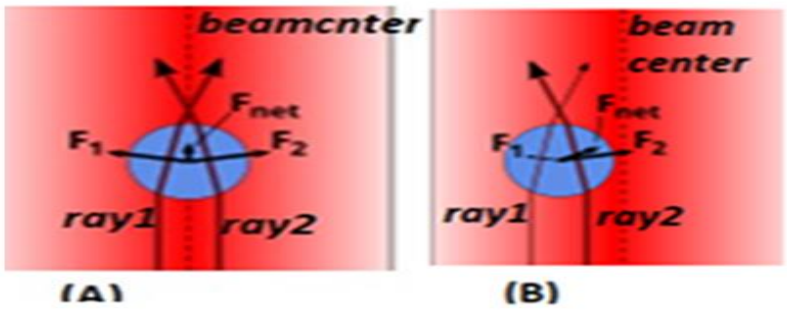

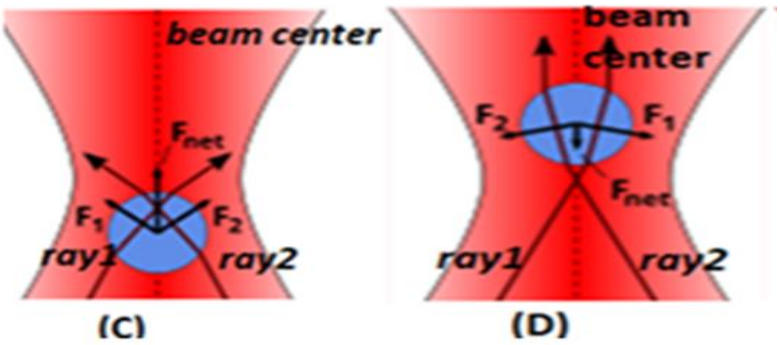

Figure 3.2 illustrates (A) when bead is focused in beam center and no net force acts on it laterally, (B) when the net force acts on bead from left side laterally (C) when the net force acts on bead from front side laterally (D) when the net force acts on bead from behind side laterally.

Generally when the newly formed focus point of the refracted rays is outside laterally or axially from true focus of the laser beam in any direction, the net force acting on the bead pushes it towards newly formed focus point.

3.4 The ways of membrane breakdown

Membrane breakdown refers to the process where the structure of a cell membrane deteriorates or disrupts. It occurs through several mechanisms such as electrophoresis, laser-induced breakdown and chemical disruption. High-intensity laser trapping can exert significant mechanical stress on the cell membrane. If this stress exceeds the membrane mechanical strength, it can lead to membrane rupture or breakdown. Local heating caused by the laser may damage the membrane by increasing the fluidity of the lipid bilayer or by directly inducing thermal stress. In some cases, the interaction of the laser with cellular molecules can lead to photochemical reactions that can contribute to membrane damage. In case of chemical disruption, chemicals like detergents or surfactants, can interacting with the lipids and proteins and solubilize them. Detergents and surfactants are amphiphilic molecules (they have both hydrophilic and hydrophobic regions with hydrophobic tails typically long hydrocarbon chains, and polar or ionic groups hydrophilic heads) as figure 3.3a below shown for sodium dodecyl sulfate (SDS) monomer. The mechanism of disruption using SDS involves three steps: (i) Detergent monomers penetrate the outer layer of the phospholipid bilayer, aligning with it according to their hydrophobic properties (see Figure 3.3a). (ii) The inserted detergent monomers induce mechanical stress on the bilayer, causing it to bend and deform (see Figure 3.3b). The hydrophobic tails of the detergent molecules interact with the hydrophobic core of the lipid bilayer, while their hydrophilic heads face the aqueous environment. (iii) As the mechanical strain increases, the bilayer reaches a critical point and forms a pore (see Figure 3.3c). This pore

further destabilizes the membrane structure and increases its fluidity, compromising the membrane's integrity [138].

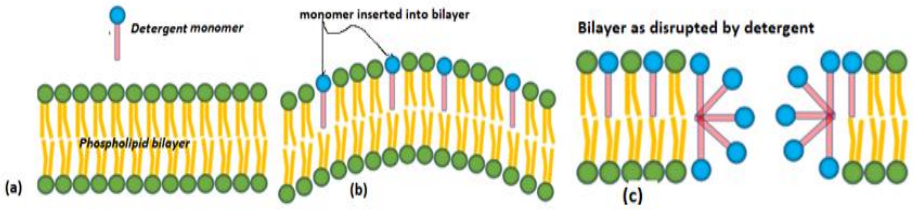

Figure 3.3 illustrates mechanism of phospholipid bilayer cell membrane breakdown by detergent as chemical disruption using sodium dodecyl sulfate.

Another mechanism of cells membrane breakdown involves using dielectrophoresis and electrophoresis techniques. Both of them are used to manipulate particles, including cells, but operate on different principles and are applied for different purposes. Dielectrophoresis relies on the interaction between particles (cells) and non-uniform electric field. When particles with dielectric property (particles that can be polarized) are exposed to spatially varying electric field, they become polarized (develop temporary dipole moments). The polarization of cells can be caused by the restricted ion motion imposed by the cell membranes. The varying field strength across the cells experiences a net force that moves the cells towards regions of higher or lower electric field strength, depends on the gradient of the electric field. In regions where the electric field changes rapidly, the force acting on the particles or cells can be significant, causing them to move toward regions of higher field strength (positive dielectrophoresis) or away from them (negative dielectrophoresis), depending on the nature of the dielectric properties of the cells relative to the surrounding medium (see figure 3.4) [138]. Additionally dielectrophoresis can be occurred as homogeneous or inhomogeneous based on the type of electric field applied on cells. It is homogeneous if electric field applied is constant (in magnitude and direction) and inhomogeneous if electric field applied varies.

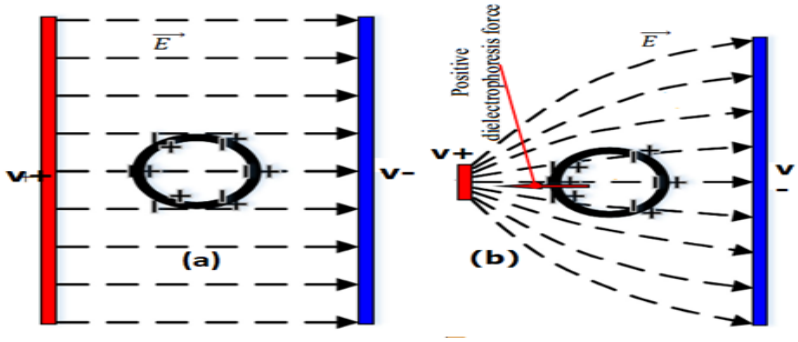

Figure 3.4 Schematic diagram of polarization in an electric field (a) Uniform electric field (b) Non-uniform electric field

Electrophoresis involves applying a high-voltage electric field to the cell membrane, creating transient pores which allow ions and small molecules to pass through the membrane. The creation of pores disrupts the cell ability to maintain normal electrochemical gradients. Ions that are normally sequestered inside or outside the cell can flow freely, leading to an imbalance in charge distribution. Particles with an electric charge move towards the electrode of opposite charge when an electric field is applied. The rate and direction of movement depend on the particle's charge and size, as well as the strength of the electric field. During electrophoresis, cells or particles are subjected to an electric field that causes them to migrate through a medium. For cells, this can result in mechanical stress due to the drag forces and electrical fields. If the electric field is strong enough, it can cause irreversible damage to the cell membrane, leading to cell lysis or breakdown as figure 3.5 [139].

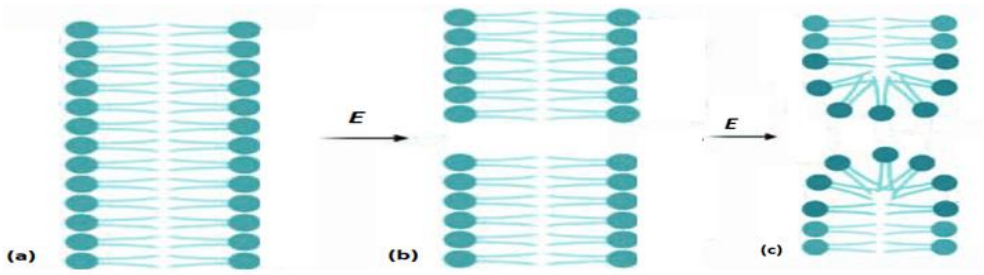

Figure 3.5 shows (a) normal cell membrane before any pore (b) cell membrane when hydrophobic pore formed by applied electric field (c) cell membrane when hydrophilic pore formed by continuous applied electric field.

In this study, the membrane of 4T1 breast cancer cells was partially damaged by a 2h treatment with DMDD. Then cells were captured and subjected to high-intensity laser radiation. The extremely strong electric field at the focal point of the laser effectively disrupted their cell membranes and prepared them for experimentation. While we used 3.1µm diameter polymer coated spherical magnetic beads to examine effect of magnetic beads on ionization of BT20 breast cancer cells.

CHAPTER 4

4. Results and Discussion

In this chapter we deeply discussed about the results and the investigations of the study. All the measured quantities such as cross-sectional areas, both before and after trapping, displacement travelled with their respective times for 4T1 breast cancer cell lines treated for two hours using Image Pro Plus6 software, and the calculated radii, volumes, and masses of the cells based on the geometric relationships between these parameters were discussed and the statistical data of these measured and calculated quantities were tabulated with descriptions. Next, an equation that describes the displacement of the cells as they moved towards the trap center is derived based on the pre-ionized dynamics of these cells. Using displacement versus time data obtained from Image ProPlus6, we fitted this equation using the Nonlinear Model Fitting function in Wolfram Mathematica12.1 and determined the unknown value of angular frequency (ω) and the charge developed on the cells. These determined values were then analyzed both statistically and graphically to explore the electrical properties of pre-ionized 2h treated 4T1 breast cancer cells as one main objective of this study. Next, we investigated the impact of magnetic beads BT20 breast cancer cell lines on their ionization properties.

4.1 Results and discussion in exploring the pre-ionized electrical properties of 2h treated 4T1 breast cancer cell lines

4.1.1 Results from measurements and calculations

Figure 4.1 below shows the captured 8 successive images of the one selected 2h treated 4T1 breast cancer cell line at different points as it travelled to the trap center. It is observable from this figure 4.1 that, as the cell entered towards the laser trap, its size decreased. This decreased in size of the cell is due to the interaction between the cell and the NIR laser that attributed to a combination of mechanical forces from optical trapping, thermal effects, changes in osmotic balance, and cellular stress responses. To make more clearable how these factors decreased the size of the trapped cell it is better to explain them orderly. (i) When a cell is trapped by the NIR laser, the laser focused the light that exerts mechanical forces on the cell, potentially leading to deformation or contraction of the cell. (ii) The trapped cell absorbs NIR radiation and the absorbed energy is converted into heat which caused increase in temperature that affect the cell cytoskeleton and membrane. This heat shrinks the cell by causing the cytoplasm to contract and by affecting cellular hydration. (iii) The exposure of the cell to NIR laser might induce a stress response in the cell that could include the activation of stress-related proteins or pathways that

alter cellular processes, such as volume regulation. This stress leads to cellular shrinkage as the cell adjusts to the stressful conditions induced by the laser. (iv) NIR laser exposure can potentially affect the permeability of the cell membrane or damage cellular ion channels and pumps, disrupting osmotic balance. This disruption leads to the loss of intracellular water and consequently causes the cell to shrink. As a whole, the NIR laser decreased the sizes of these breast cancer cells when they interact with it by the above mechanisms. So, as the cells approached towards its center from outside they show gradual reduction in size (see figure 4.1 a to h). Image 4.1, (a) shows the cell before trapped which has the largest size and (h) shows the cell after trapped and in the trap center which has the smallest size.

To emphasize this reduction in size of the cells to the actions of the laser trapping, I have measured the areas 18 cells both before and after trapped using the software Image pro Plus6 in units of pixels by the assumption that all these 2 h treated 4T1 breast cancer cells analyzed in this study are spherical in models. Then we computed the areas of these cells in meters by using the conversion factor $7.27 \times 10^{-8} meter/pixel$, which was determined using 3.1 μm silicon beads. Then based on the basic geometrical relationships between them, we calculated radii and volumes of these cells both before and after trapped.

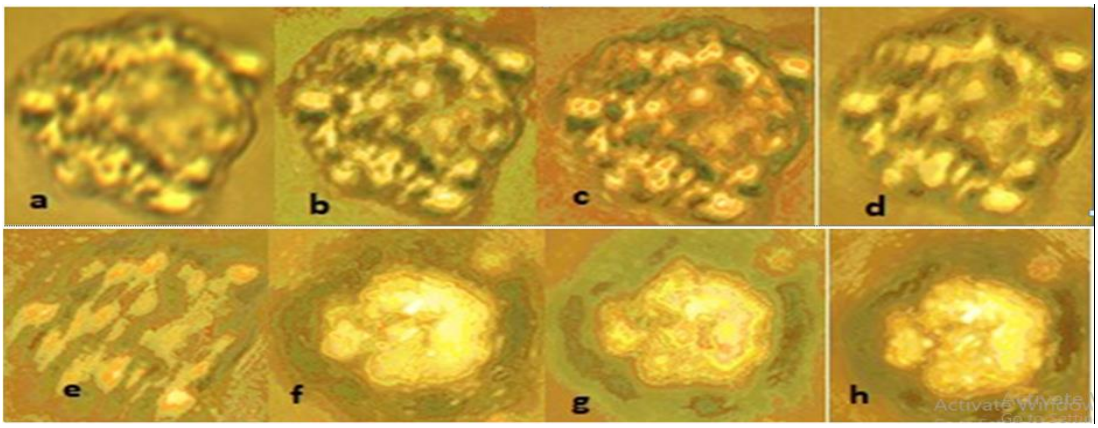

Figure 4.1 shows the 8 captured successive images of the one selected 2h treated 4T1 breast cancer cell as it moved to the trap.

Additionally, the masses of cells were calculated, both times, from the definition of density as, $m_{\text{cell}} = \rho_{\text{cell}} \times V_{\text{cell}}$, where the known density of the 4T1 breast cancer cells is 1081 kg/m^3. The statistical data of these quantities was illustrated in the table 4.1 below for both before and after trapped.

Quantities	2h treated 4T1 breast cancer cells before trapped (18)				
	Mean	St. Deviation	Min	Median	Max
$R_{\text{cell free}}$ (μm)	70.6418	14.61301	38.5394	73.64865	93.67092
$A_{\text{cell free}}$ (mm^2)	0.0163	0.00606	0.00466	0.01703	0.02755
$V_{\text{cell free}}$ (mm^3)	0.00165	0.000841	0.00024	0.00167	0.00344
$m_{\text{cell free}}(ng)$	1.77957	0.9098	0.25907	1.80802	3.7197
	2h treated 4T1 breast cancer cells at the center of trap (18)				
$R_{\text{cell trap}}$ (μm)	67.596	15.26352	33.7522	71.58962	90.16658
$A_{\text{cell trap}}$ (mm^2)	0.01504	0.00594	0.00358	0.01609	0.02553
$V_{\text{cell trap}}$ (mm^3)	0.00147	0.000781514	0.00016	0.00154	0.00307
$m_{\text{cell trap}}$ (ng)	1.58768	0.84482	0.17402	1.66068	3.31765

Table 4.1 shows the statistics of measured areas and calculated values of radii, volumes and masses the 2h treated 4T1 breast cancer cells.

These cells have 70.64±14.61 μm, 0.0163±0.006 mm^2, 0.00165±0.0008 mm^3 and 1.77±0.90 ng average radius, area, volume, and mass respectively before trapped, and 67.59±15.26 μm, 0.0150±0.0059 mm^2, 0.00147±0.00078 mm^3 and 1.58±0.84 ng average radius, area, volume, and mass respectively after trapped. To demonstrate the reduction in size of these cells, we calculated their difference in volume and the resulted average reduction in volume was about 13.48±7.93%, which shows countable decreased in size of the cells.

4.1.2 The pre-ionized dynamics of 2h treated 4T1 breast cancer cells

To determine the magnitude of the charge developed on 2h treated 4T1 breast cancer cells and the stiffness of the laser we focused on analyzing the pre-ionization dynamics of individual cells. We began by solving the equation of motion for vector $\vec{r}(t)$, which describes the displacement of the cell over time as the cell travelled to trap center. Then the charge developed on each cell is determined by fitting the displacement versus time data recorded and assumed a variable (unknown) angular frequency using the nonlinear curve fitting model of Wolfram Mathematica12.1. Then from the calculated mass of the cell and determined angular frequency from fitting, we computed the value of the trap coefficient (stiffness).

As cells moved into the laser trap, they become polarized by the laser electric field, generating polarization charges. These charges create an induced electric field that opposes the applied electric field from the laser, reducing the net trapping force. Both the induced electric field and dipole moment oscillations increase as the cells approached to the trap center, further decreasing the effectiveness of the trapping force. Additionally the strong electric field near the trap center (primarily due to the specific arrangement of electrodes and the high voltages applied to them, which create a concentrated and intense electric field in that region), disrupts dipole oscillations and generating free charges. These free charges produce a Coulomb force that opposing the trapping force. Thus the Coulomb force repels the cells or resists their movement, leading to a decrease in cell velocities. In addition to the free charges generated from disruption of dipole oscillations and polarizations, the membrane breakdown of the 2h treated 4T1 breast cancer cells, those treated with 2-dodecyl-6-methoxycyclohexa-2, 5-diene-1, 4-dione (DMDD) compound, also developed the charge. So, the total developed charge is the summation of all these charges. The actions of these opposing forces generally disturb the cells travel to the trap center including their displacements. Consider table 4.2 below.

Quantities	2h treated 4T1 breast cancer cells (18)				
	Mean	St. Deviation	Min	Median	Max
$r_{cell}(\mu m)$	4.78827	25.45317	0	0.87713	241.75076
$v_{cell}(\mu m/s)$	27.13165	98.03879	0.57258	7.88891	726.137
$a_{cell}\,(\mu m/s^2)$	55.30079	255.13785	-492.173	12.5772	1760
$t_{cell}(s)$	0.26183	0.19566	0	0.2504	0.8

Table 4.2 shows the statistics of displacements, times, velocities and accelerations where r is displacement (μm), v is velocity ($\mu m/s$), a is acceleration (μm/s^2) and t is time (s).

The average displacement and time taken were 4.78±25.45 μm and 0.26±0.19 s respectively. These results illustrated that the cells were speeding up firstly up to some points and then started to slow down as they approached the trap center. This is due to two main reasons: (i) the induced electric field that decreased the trapping force and (ii) the breaking down of dipole oscillations by strong electric field near the trap that generate the free charges, resulting in creation of Coulomb force which repels the cells or resists their movement towards the trap center. Graphically this idea is demonstrated by displacement versus time graph of the cells as shown by the figure 4.2 below. As it can be observed from the violet line on figure 4.2 that, the cells were speeding up initially for some points (up to the black dotted pointed on the violet line) and then began to slowing down as they approached to the trap center due to the reasons mentioned above. Their displacements varied from 0 μm to 241.75 μm as explained in table 4.2 with average value of 4.78 ±25.45 μm.

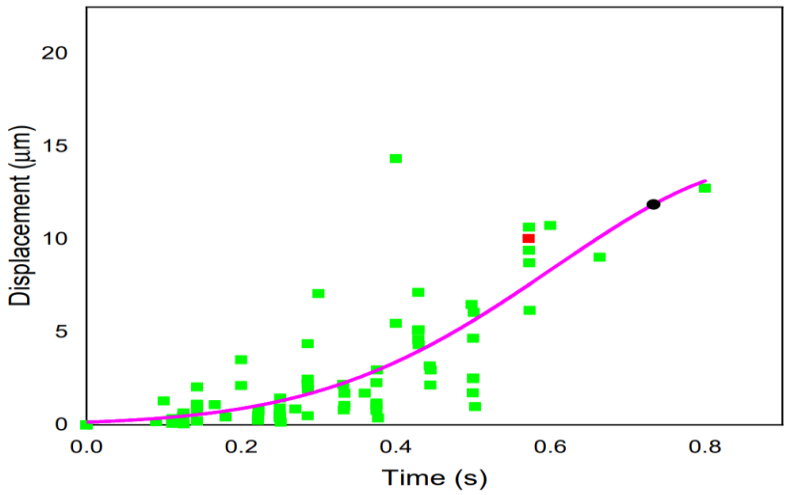

Figure 4.2 illustrates the displacement-time graph of the pre-ionized 2h treated pre-ionized 4T1 breast cancer cells.

The velocities and accelerations of the cells were computed from first and second derivatives of the displacement versus time data recorded respectively using Origin Pro2019b. When we differentiated the displacement versus time data above, using software Origin pro2019b, the velocities of the cells can be determined. The velocity versus time graph of these 2h treated pre-ionized 4T1 breast cancer cells was shown by figure 4.3 below.

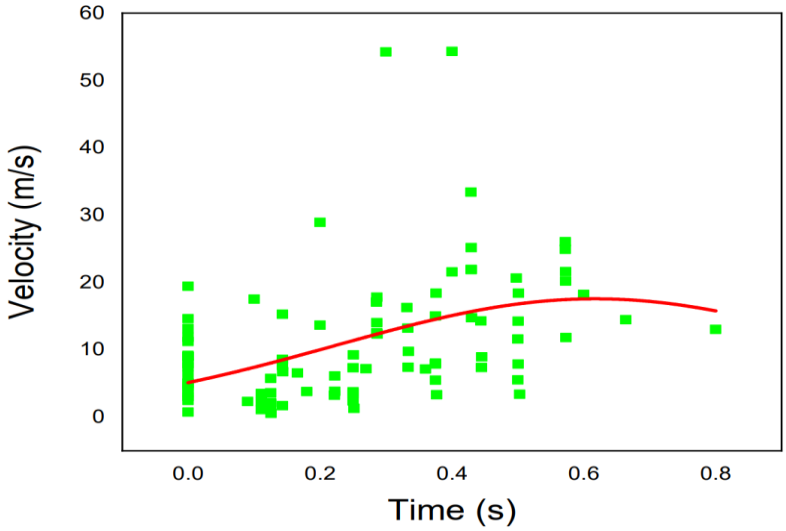

Figure 4.3 the velocity versus time graph of the pre-ionized 2h treated 4T1 breast cancer cells as they moved to the trap center.

The graph on figure 4.3 illustrates that the velocities of the cells increased for some point as cells travelled to the trap up to reach maximum point of 726.13 $\mu m/s$ before they become influenced by the opposing generated electrostatic forces and then decreased as they approached towards the trap center because of these opposing forces as indicated by red line. The decreasing in these velocities continued up to they totally trapped in the trap center. In magnitude the velocities of these cells varied from 0.57 $\mu m/s$ to 726.13 $\mu m/s$ with average value of 27.13±98.03 $\mu m/s$ as tabulated in table 4.2.

If the above differentiating is repeated once, the accelerations can be obtained for the 2h treated pre-ionized 4T1 breast cancer cells. When drawn to graph, the acceleration versus time graph was shown by figure 4.4 below.

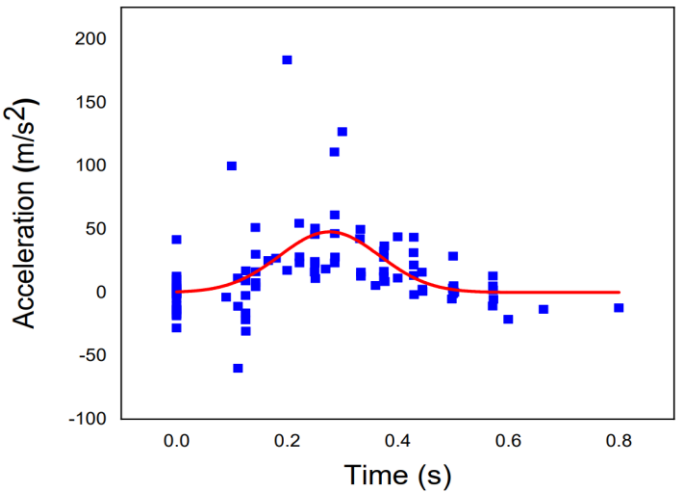

Figure 4.4 illustrates the acceleration-time graph of the pre-ionized 2h treated 4T1 breast cancer cells.

This graph again illustrates that initially these cells were accelerated up to they reached maximum acceleration (peak point) before started to oppose by the induced electrostatic force as they approached to trap center. After this maximum point the cells decelerated and finally entered to the trap deadly as indicated by red line. The acceleration of these cells varies from -492.17 μm/s^2 to 1760 μm/s^2 and average value of 55.30 μm/s^2.

The Forces

Motion of the breast cancer cells as they moved to the laser trap is influenced by the actions of three basic forces. These fundamental forces acting on the trapped cells are electrostatic, drag and trapping forces. Their origins and how they act on these cells are described below.

1. Trapping force is generated by an optical trap or optical tweezers, which use a focused laser beam to create a potential well for trapping and manipulating particles or cells. Its magnitude depends on the size of the cells and the rate of change of displacements of the cells with time, the strength of the electric field (increasing as the cells are moving towards the trap center and decreasing away from center of the trap), and the cells dielectric susceptibility (refers to how they polarize in response to the electric field of the laser). This polarization affects how the cells interact with the laser light, which in turn influences the trapping force. Trapping force always attract the cells towards its center. It is given by equation;

$$F_t(r) = kr \tag{4.1}$$

where r is the displacement of each cell, and k is the constant known as trap coefficient which is a crucial parameter that quantifies the strength and effectiveness of the trapping force exerted by the laser trap on a cell. It depends on several factors, including the intensity and properties of the laser, the optical properties of the trap, and the dielectric properties of the cell. It is directly proportional to the laser power (as the power increases, the intensity of the laser beam at the focus increases, leading to a stronger electric field and a higher trap coefficient). The size and shape of the cells affect their interaction with the electric field. Larger cells or those with irregular shapes can experience different trapping forces compared to smaller or more spherical cells. For spherical cells, the trapping force scales with the cell volume.

2. Electrostatic force is another important force acts on the trapped cells, generated from charges developed by ionized cells and acts against the trapping force. When cells entered in to the trap, the electromagnetic field radiations are ionized them. As a result of the membrane breakdown the charge is developed. This developed charge depends on the extent at which the cell membrane breakdown and the area of each cell. The raised the value of developed charge the increased in magnitude of electrostatic force. From the basic relationship between electric charge, electric field strength and electrostatic force, the electrostatic force acting on the 2h treated 4T1 breast cancer cell can be determined as;

$$F_{\mathrm{e}}(r) = qE_0 \tag{4.2}$$

where q is the magnitude of charge accumulated on each cell and E_0 is the maximum value of electric field, known as electric field amplitude, can be determined as,

$$E_0 = \sqrt{\frac{2P}{A\varepsilon_2 v}} = \sqrt{\frac{2P\mu_0 v}{A}} \tag{4.3}$$

where P is the power measured at trap position (0.806W), v is the speed of light in the medium that the cell is suspended in (FBS), μ_0 is the free space magnetic permeability, and $A = \pi w^2$, is the beam area (size) computed from the beam radius ($w = 243.2\mu m$) at the back of objective lens with its numerical aperture (1.25). With these values the electric field amplitude is,

$$E_0 = \sqrt{\frac{2\times 0.806\times 3\times 10^8\times 4\times 10^{-7}}{1.33\times (243.2\times 10^{-6})^2}}$$

$E_0 = 49.58kV/m$, from the relationships between speed of light in free space (c), speed of light in medium (v), and refractive index of the medium (n_{m}) , $n_{\mathrm{m}} = c/v$ ($n_{\mathrm{m}} = 1.33$ for FBS) and from the relation again, $c = 1/\sqrt{\mu_0\varepsilon_0}$, where ε_0 is permittivity of free space.

3. Drag force is the other force acts on 2h treated 4T1 breast cancer cells as they moved to the trap. It is the opposing force arises from the surface of the medium in which the cells are suspended and depends on the radius of the cell (R), assuming that all the 2h treated 4T1 breast cancer cells are spherical in models with radius R, and rate of change of displacement with time. Based on these facts the drag force can be determined using equation,

$$F_d = 6\pi\mu R\frac{dr}{dt} \qquad 4.4$$

where μ is the fluid viscosity that the cell is suspended in, FBS ($\mu = 1.02\times 10^{-3}Ns/m$). Depending on the values of the three forces the resultant force acting on the 4T1 breast cancer cells as they move toward trap center can be generalized by the following equation,

$$F_{net} = F_t - F_d - F_e \qquad 4.5$$

which has the form of the Newton's second law, $F_{\mathrm{net}} = ma = m\frac{d^2r}{dt^2}$. When their values are substituted from Eq.4.1, Eq.4.2 and Eq.4.4, the net force becomes,

$$m\frac{d^2r}{dt^2} = kr - 6\pi\mu R\frac{dr}{dt} - qE_0 \qquad 4.6$$

When Eq.4.6 is rearranged we can get,

$$m\frac{d^2r}{dt^2} + 6\pi\mu R\frac{dr}{dt} - kr = -qE_0 \qquad 4.7$$

which has the damped harmonic oscillator equation form. Again by more rearrangement it can be,

$$\frac{d^2r}{dt^2} + \frac{6\pi\mu R}{m}\frac{dr}{dt} - \frac{k}{m}r = -\frac{q}{m}E_0 \qquad 4.8$$

If the coefficients of the drag force and the trapping force of Eq.4.8 are represented by other constants as, $\gamma = \frac{3\pi\mu R}{m}$ and $\frac{k}{m} = \omega^2$ 4.9

where the value of the constant γ varies with radii and masses of the cells, ω is the angular frequency and m is mass of each cell before trapped. Then the simplified form of Eq.4.8 is the next;

$$\frac{d^2r}{dt^2} + 2\gamma\frac{dr}{dt} - \omega^2 r = -\frac{q}{m}E_0 \qquad 4.10$$

where r is the displacement of the given cell as it travels to the trap center. Eq.4.10 is the second order inhomogeneous differential equation that can have homogenous and particular solutions. So its general solution is the summation of the two solutions. The homogeneous part has the form;

$$\frac{d^2r}{dt^2} + 2\gamma\frac{dr}{dt} - \omega^2 r = 0 \qquad 4.11$$

with solution of the following form;

$$r_{\mathrm{h}}(t) = e^{-\gamma t}(Ce^{\sqrt{\gamma^2+\omega^2}t} + De^{-\sqrt{\gamma^2+\omega^2}t}) \qquad 4.12$$

where constants C and D can be determined from the initial conditions. Then the particular equation has the form;

$$r_{\mathrm{p}}(t) = Ab \qquad 4.13$$

In Eq.4.13 $r_p(t)$ is constant which has no first and second derivatives and A is the coefficient of b. If the value of coefficient A be determined and $A = 1/\omega^2$, then we get the particular solution that looks like;

$$r_p(t) = \frac{1}{\omega^2} \times \frac{q}{m} E_0 = \frac{q}{m\omega^2} E_0 \qquad 4.14$$

By the next, the general solution that represents the displacement of the 2h treated 4T1 breast cancer cell becomes,

$$r(t) = e^{-\gamma t}\left(Ce^{\sqrt{\gamma^2+\omega^2}t} + De^{-\sqrt{\gamma^2+\omega^2}t}\right) + \frac{q}{m\omega^2} E_0 \qquad 4.15$$

As mentioned above, values of constants C and D in Eq.4.15 can be determined from initial position and initial velocity of the cell at initial time $t_0 = 0$. Then when we substitute their values into Eq.4.15, the equation for the displacement of the 4T1 breast cancer cells becomes;

$$r(t) = e^{-\gamma t}\left(\frac{q}{2m\omega^2} E_0\left(-1 - \frac{\gamma}{\sqrt{\gamma^2+\omega^2}}\right) e^{\sqrt{\gamma^2+\omega^2}t} + \frac{q}{2m\omega^2} E_0\left(\frac{\gamma}{\sqrt{\gamma^2+\omega^2}} - 1\right) e^{-\sqrt{\gamma^2+\omega^2}t}\right) + \frac{q}{m\omega^2} E_0,$$

and after simple we made some rearrangements,

$$r(t) = \left[-\frac{q}{2m\omega^2} E_0\left(e^{\sqrt{\gamma^2+\omega^2}t} - e^{-\sqrt{\gamma^2+\omega^2}t}\right) - \frac{q}{2m\omega^2} E_0 \frac{\gamma}{\sqrt{\gamma^2+\omega^2}}\left(e^{\sqrt{\gamma^2+\omega^2}t} - e^{-\sqrt{\gamma^2+\omega^2}t}\right)\right] + \frac{q}{m\omega^2} E_0 \qquad 4.16$$

From the mathematical relations, $\frac{1}{2}\left(e^{\sqrt{\gamma^2+\omega^2}t} + e^{-\sqrt{\gamma^2+\omega^2}t}\right) = cosh\sqrt{\gamma^2+\omega^2}t$ and $\frac{1}{2}\left(e^{\sqrt{\gamma^2+\omega^2}t} - e^{-\sqrt{\gamma^2+\omega^2}t}\right) = sinh\sqrt{\gamma^2+\omega^2}t$. Finally the result of Eq.4.16 becomes,

$$r(t) = \frac{q}{m\omega^2} E_0[1 - e^{-\gamma t}\left\{cosh\sqrt{\gamma^2+\omega^2}t + \frac{\gamma}{\sqrt{\gamma^2+\omega^2}} sinh\sqrt{\gamma^2+\omega^2}t\right\}] \qquad 4.17$$

Equation 4.17 describes how the displacements of the cells change over time as they move from their initial free positions to the center of the trap. This equation represents an over damped harmonic oscillator (non-oscillatory, exponential nature of the cells response to the driving force), where electrostatic force is the driving force, drag force is damping force and trapping force is restoring force, as indicated by Equation 4.10. Also the use of hyperbolic functions (cosh

and sinh) confirms that the cell motion is characterized by exponential decay (not oscillatory) behavior) during its motion towards the laser trap and undergoes over damped motion because the damping is strong enough to prevent any oscillatory behavior, resulting in the hyperbolic solution form.

Based on Equation 4.9, the drag coefficient (γ) for each cell can be determined, and it ranges from 241.96 Ns/kg to 1429.37 Ns/kg, with average value of 503.37 ± 302.66 Ns/kg (table 4.3 below). This variation depends on the radius and mass of the cells, with the drag coefficient increasing with the cell radius and decreasing with the cell mass. Then using the value of electric field amplitude ($E_0 = 49.58\, kV/m$), the average beam radius ($w = 243.2\, \mu m$), the masses of each cells, the value of γ calculated for each cell, and the measured displacements vs time data, we fitted Eq.4.17 using Wolfram Mathematica12.1 Nonlinear model fitting function at 0.99 confidential level to determine the two unknown quantities, the developed charge (q) and angular frequency (ω), of each 2 h treated 4T1 breast cancer cells. In fitting this equation simultaneously to determine both q and ω we used the value of R-squared, R^2 (agreement of determination) that varied from 0.99902 to 0.99994 with average value of 0.99955±0.000248 and observed that the value of charge developed (q) on cells are all negatives, indicates that the electric field (applied laser field) is attracting the negatively charged cells and the induced field is opposing their motion towards the trap. Next, based on their sizes we expressed these generated charges in terms of z-number as, $z = \frac{q}{e} = q/(1.6 \times 10^{-19}c)$, where q is the magnitude of charge developed on each cell and e is the magnitude of elementary charge. Based on the extent at which the cell membrane is breakdown and radius of the cells, the charge developed on cells was different from cell to cell. As the cell membrane breaks down, it can alter the cell interaction with the electric field. Greater membrane breakdown may increase permeability (ionic conductivity), leading to changes in charge distribution and affecting the amount of charge the cell can develop. While a larger cell radius can increase the charge accumulation due to a larger interaction surface with the electric field. Using the determined values of angular frequencies and masses of the cells, we also calculated the value of trap constant based on Eq.10.9. The statistics of developed charge (q) on cells in terms of z-number, angular frequency determined (ω), trap constant (k) and drag coefficient (γ) calculated for each cell using Eq.4.9 above, is shown by table 4.3 below.

Quantities	2h treated 4T1 breast cancer cells (18)				
	Mean	St. Deviation	Min	Median	Max
$\gamma\ (Ns/kg)$	503.37275	302.66976	241.96215	391.41862	1429.37415
$\omega(rad/s)$	72.12849	30.12239	24.6218	69.1882	156.601
k(μN/m)	8.32901	4.55411	0.310917	7.32182	17.3458
z-number	432.60156	688.77186	2.98311	184.03312	2902.91875

Table 4.3 shows the statistics of calculated γ, z and determined ω of the pre-ionized 2 h treated 4T1 breast cancer cells.

The values of calculated z-numbers for the developed charges were ranged from 2.98 to 2902.91 with average value of 432.60±688.77 and this high difference is because of dependency of the charge generated on the size (radius) of the cell. It is directly proportional the size of the cell (i. e the larger the size of the cell the greater the charge developed on it). This also indicates the greater the size (surface) of cell the greater the laser interacts with it and the charge developed. Figure 4.5 below illustrates the proportionality between size (radius) of the cells and charges developed on them as shown by red line.

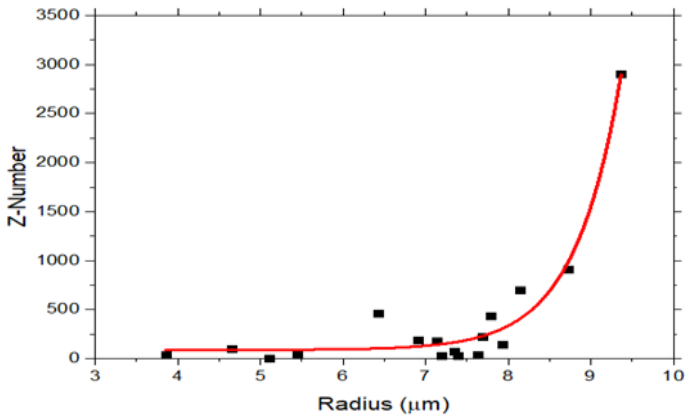

Figure 4.5 shows the charge developed on pre-ionized 2 h treated 4T1 breast cancer cells versus radius of the cells.

Another key point we observed from fitting Eq. 4.17, aside from determining the value of angular frequency (ω), is its relationship with developed charge on the cells. The figure 4.6 below demonstrates how developed charge on pre-ionized 2 h treated 4T1 breast cancer cells related to the angular frequency determined for these cells from fitting function above.

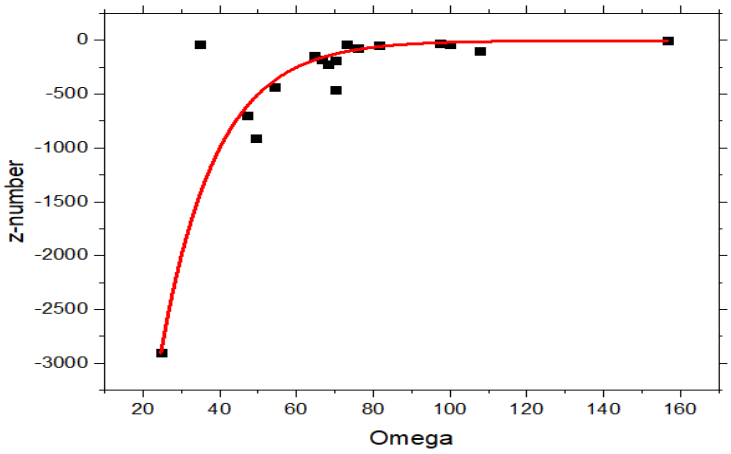

Figure 4.6 shows the relationship between z-number of pre-ionized 2 h treated 4T1 breast cancer cells and their angular frequency.

Figure 4.6 above shows that developed charge, in z-number, and angular frequency have positive relationships; but they do not increasing equally at all points as the cells moved to the trap center. Initially as the cells moved to the trap the developed charge increased rapidly due to the electromagnetic field of the laser up to the cells reached near the trap, where the induced electrostatic force oppose their motion. While the angular frequency increased slowly due to the cells were linearly accelerating rather than vibrating that resulted from the higher attraction of trapping force and lower stressed of the cells from electrostatic opposing. After that as they approached to the trap center, the opposition of the induced electrostatic force increased, as result the cells were stressed and became vibrating which causes the increasing in angular frequency of them as shown by red line on figure 4.6 above. This in-depth relationship between the z-number and angular frequency highlighted how the dynamics of the charged cells evolve as they interact with electric field. Understanding this relationship is important for optimizing conditions in applications like targeted therapies or cell manipulation techniques. The determined angular frequency of these cells has the value ranged from 24.62 rad/s to 156.60 rad/s with average value of 72.12±30.12 rad/s and the calculated value of trap coefficient from the mass of each

cells and determined angular frequency, using Eq.4.9, has value that varies from 2.98 μN/m to 17.34 μN/m with average of 8.32±4.55 μN/m.

4.2 The effect of magnetic beads on ionization property of BT20 breast cancer cells

When BT20 breast cancer cell is exposed to the laser field, laser trap use focused laser beam to capture and hold the cell. As the cell stays in the laser trap, it absorbs infrared radiation. This leads to ionization through mechanisms such as increasing the cell thermal energy or directly through interactions with the laser field (dipole-electric interactions between the cells and the trapping field generated by the infrared laser radiation).

As demonstrated by Kelley, Gao, and Erenso (2016), the ionization period for a given amount of infrared radiation incident on these BT20 cells alone is averaged to about 8 minutes [122-123]. This ionization period refers to the time interval between the moment at BT20 breast cancer cell is captured by the laser trap and the point at which it is ejected from the trap due to Coulombic repulsion. Essentially, this period measures how long it takes for the cell to be ejected from the trap after it begins accumulating charge. This repulsion occurs as a result of the progressive build-up of charge on the cell. As the cell absorbs infrared radiation, it gradually accumulates charge, which increases the electrostatic forces acting on it. Once the accumulated charge reaches a threshold where the Coulombic force (the electrostatic force between the charged cell and the trap) becomes strong enough, the cell is ejected from the trap.

By inserting magnetic beads in to the cells, we aimed to investigate their impact on ionization period and observe changes in cells behavior. To collect the cells ionization data, we measured the displacement, speed, and time for each BT20 cell and magnetic bead entering and exiting the trapping zone. Using Image proplus6 software, the center of origin was positioned at the center of the BT20 cell during its initial trapping. Then we convert pixel measurements into micrometers, using the known diameter of 3.1μm of the magnetic beads as the calibration standard. Data points were then plotted to track the movement of the cell or magnetic bead as they entered and exited the laser trap. For each plotted point, the software recorded the horizontal and vertical positions, their respective speeds, and the corresponding times.

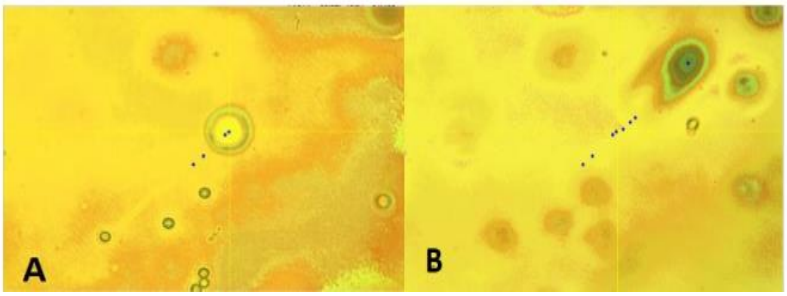

Figure 4.7 shows the data analysis process for measuring the displacement, speed, and time of the BT20 cell using Image prop lus6. The blue dots represent the plotted data points showing the cell movement as it approached and exited the laser trap. The intersection of the yellow x and y lines marks the center of origin. Panel (A) displays the data points recorded before the cell entered the trap. Panel (B) shows the data points recorded before trapped and after exited the trap.

In Excel 2010, the data was categorized into two groups: before trapping and after exiting the trap. Additionally, an equation was developed to calculate the total displacement by combining the horizontal and vertical positions recorded by Image pro. The average speeds of the three selected cells, 3.3 μm/s, 2.9 μm/s, and 10 μm/s when entering and 5 μm/s, 12 μm/s, and 34 μm/s when exited the trap respectively, as illustrated by figure 4.8 below.

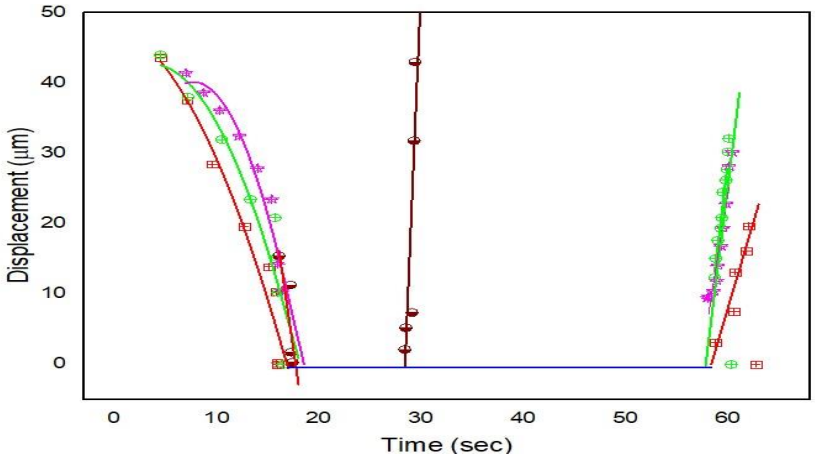

Figure 4.8 shows the displacement versus time for each of the three selected cells.

Figure 4.8 displays that when the laser port is opened, each cell (red, green, and brown) accelerated towards the center of the trap (as shown by the trajectories on left sides), then stayed in the trap (shown by the horizontal blue line) and ejected from the trap at higher speeds as (shown by the steep sloping straight lines). The ionization period (duration of the cells stayed in the trap) is almost similar for the two cells (red and green) about 42 seconds and about

11seconds for one cell (shown in brown). Once here, a variation of duration they stayed in the trap observed from results of the ionization periods of the same types of cells (all are BT20 cell lines) is raised from factors such as size, shape (irregularity), charge-to-mass ratio, cellular density (stiffness), intracellular content (such as different levels of proteins, lipids, or organelles). As a whole, the insertion of the magnetic beads highly reduced the ionization period of these cells in comparison with the periods of the BT20 cells without magnetic beads demonstrated previously [122-123]. The reduction in this ionization period was as high as about 83% which confirmed the Erenso et al. (2024) illustration [124].

A series of snapshots describing the trajectory of the brown cell (shown in Figure 4.8) is presented in Figure 4.9 below. It shows snapshots of the cell as it moved through different phases: approached to the trap (blue), stayed in the trap (black), and being ejected from the trap (green).

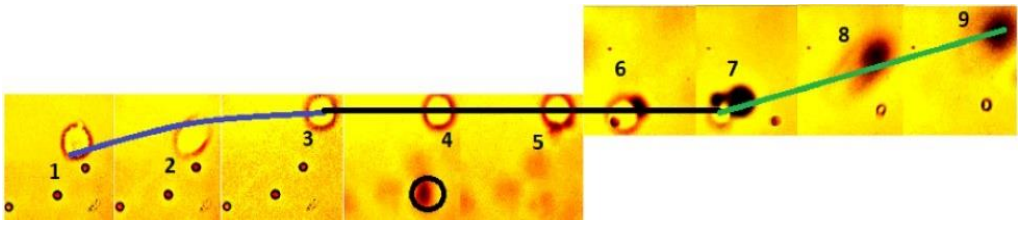

Figure 4.9 shows a sequence of snapshots illustrating the cell's trajectory as it moved into, stayed in and subsequently ejected from the trap.

The first three snapshots display magnetic beads (indicated by black circles) adhering (sticking) to the slide. Once the cell entered the trap (in the third snapshot), a magnetic bead accelerated toward the trap (because the trap creates a localized magnetic field that influences the movement of nearby magnetic beads, magnetic field exerts a force on the bead, causing it to move more quickly toward the trap) and attaches to the cell (snapshots 4-6). This attachment created a small dark region, which can be enlarged as the bead continued to interact with the cell and is the indicative bead influence on the cell environment (snapshot 7), just before the cell is ejected. In other words, as the bead accelerated towards the trap and attached to the cell, the local environment around the cell (such as changing in the cell structure or its surrounding medium, movement or concentration of ions, mechanical stress) is disrupted. This altered the cell ionization properties and leading to a shortness of ionization period. The faster the beads interact with the laser fields, the faster the cells environment disturbed and the larger formation of the dark region. The graph on figure 4.10 below illustrates the rate at which the area of the dark region formed on five selected cells (yellow, dark yellow, black, blue and pink lines) increased with time before the cells being ejected from the trap.

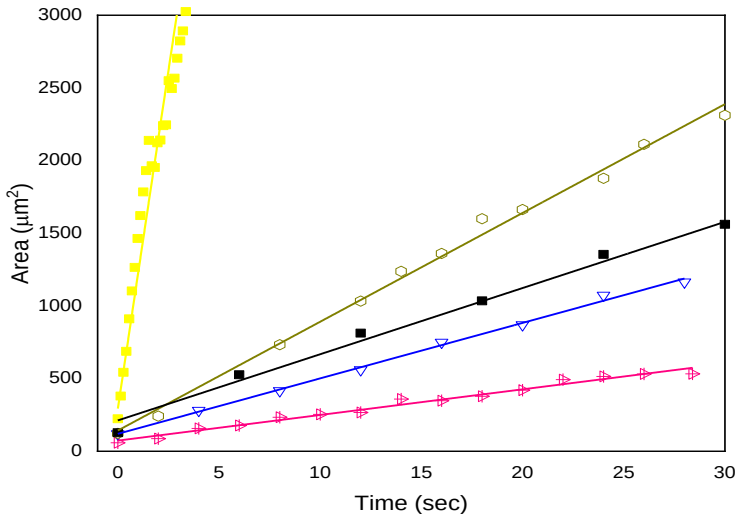

Figure 4.10 illustrates how area of the formed dark region related to time the beads stayed in the trap where area measured is in μm^2 and time is in seconds.

On average the rate of expansion of this formed dark region for the five selected cells were about 1032 $\mu m^2/s$ for yellow, 86 $\mu m^2/s$ for dark yellow, 74 $\mu m^2/s$ for black, 46 $\mu m^2/s$ for blue and 22 $\mu m^2/s$ for pink line. The difference in rate of expansion of the dark region is resulted from the difference in interaction extent of the beads with laser fields which was affected by the physical and chemical properties of the cells. The cell shown by yellow line interacted quickly with magnetic beads so that it has the greatest rate of the dark region expansion, while the cell shown by pink line interacted slowly with magnetic beads and has the least rate of the dark region expansion. Generally the faster the cells interacted with the beads the greater the rate at which the dark region expanded due the cells environment disrupted quickly.

As the beads are ejected from the trap, the initially created dark region diminished because the beads influence have no longer disturbance and this resulted in increasing brightness (light emission). As demonstrated in figure 4.11 below, the greater the ionization extent leading to greater brightness.

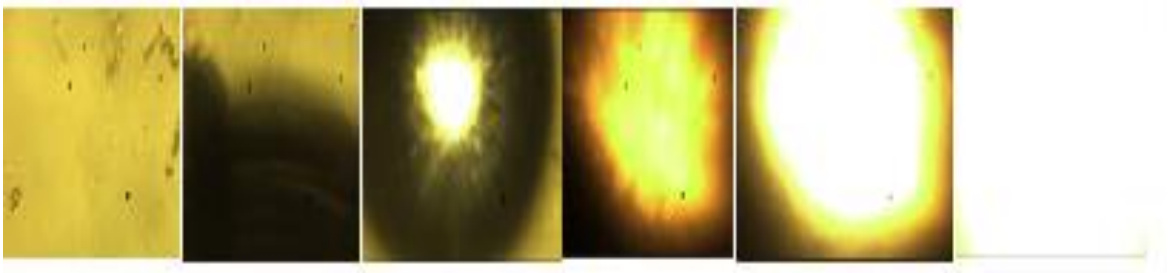

Figure 4.11 illustrates the successive snapshots that show increasing of the brightness with increasing ionization extent of selected BT20 breast cancer cell line as it moved away from the laser trap. The third snapshot (from left to right) shows where the cell is started ejecting and ionizing, and brightness increased rapidly.

The trajectories of the beads as they were ejected from the trap are depicted in Figure 4.12(a), with the trap is at the origin of the x-y coordinate system. These trajectories illustrate how the surrounding environment such as the Earth magnetic field and thermophoretic forces impacted the movement of the beads away from the trap and followed diverging paths. Initially as these beads ejected from the trap, their displacements were high (both in magnitudes and directions) due to the pushing force from the trap. But, as these beads moved away this pushing force decreased, and the Earth magnetic field and thermophoretic forces influenced their paths.

Magnetic beads possess magnetic moments and will be aligned with the Earth's magnetic field lines. This caused the beads to deviate from their expected paths as the field alignment conflicted with their trajectories of post ejection due to this Earth's magnetic field exerted a Lorentz force on magnetic beads with residual magnetic moments, resulted in deflection of the beads trajectories, potentially bending or altering their paths away from a straight line or intended direction. In addition to Lorentz force applied by it, local variations in the Earth magnetic field also created gradients (distortions) that further affect the trajectories of the beads and cause additional deviations or irregularities in beads movements.

The other force that influenced the trajectories of the beads is the thermophoretic force, which resulted from the difference in local thermal energy generated by the NIR laser when it created a localized heating effect. This force produced by temperature gradient pushed away the beads from the laser focus towards cooler areas, leading to curved or shifted from the original path dictated by the laser trap alone and more significant deviations. Generally, the combined effects of these forces made complex trajectories of these beads as shown on figure 4.12(a) below.

The Earth magnetic field and the thermophoretic force affected not only trajectories of the beads but also they affected their speeds. Initially these beads ejected from the trap with high speeds and in their own directions because of the pushing electrostatic force from the trap. But, later their speeds disturbed by the combination influence of the Earth magnetic force and the thermophoretic force. The thermophoretic force accelerated or decelerated them towards the lower temperature gradient, whereas the Earth's magnetic field caused adjustments in speeds due to magnetic drag. These resulted in the complexities of speeds of the beads as on figure 4.12(b) below.

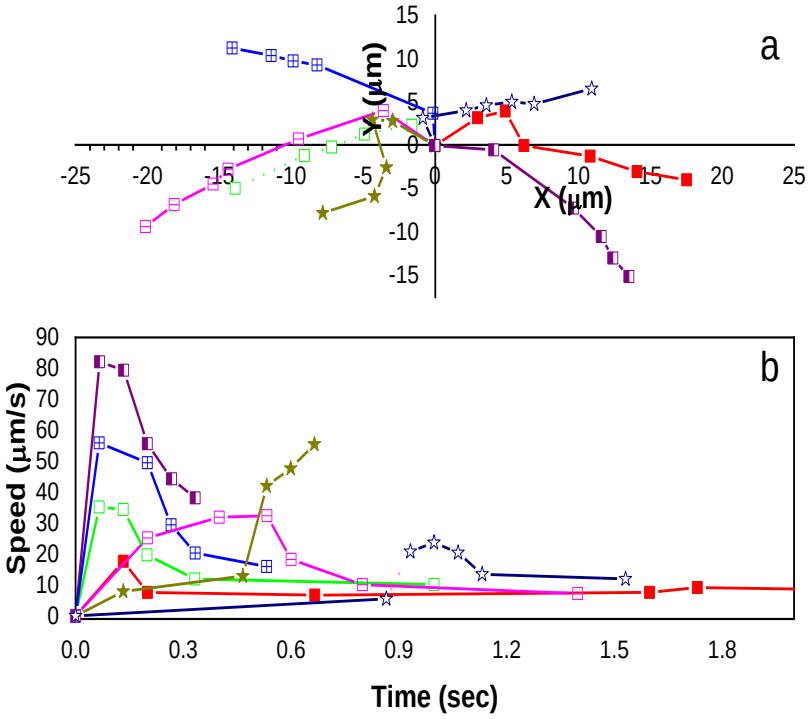

Figure 4.12 shows (a) the trajectories of the beads as they ejected from the trap, (b) how the speed of the beads changed over time after ejected from the trap.

CHAPTER 5

5. Conclusion and Recommendation

5.1 Conclusion

The measurements of cell areas before and after trapping, as well as the calculation of various parameters such as radii, volumes, and masses of these cells were presented and the statistical data of these quantities were tabulated with detailed descriptions. These parameters have, 70.64±14.61 μm, 0.0163±0.006 mm^2, 0.00165±0.0008 mm^3 and 1.77±0.90 ng average radius, area, volume, and mass respectively before trapped, and 67.59±15.26 μm, 0.0150±0.0059 mm^2, 0.00147±0.00078 mm^3 and 1.58±0.84 ng average radius, area, volume, and mass respectively after trapped which their difference indicated the reduction of the cells size with about 13.48±7.93%, resulted from actions of the optical trapping force.

The equation that describes the cells displacement as they move towards the trap center was derived, based on their pre-ionized dynamics. Then this equation is fitted to the measured displacement versus time data using Nonlinear Model Fitting in Wolfram Mathematica12.1 to determine the angular frequency (ω) and cell charge. Using these values, the trap coefficient (stiffness, k) was calculated. The average values of charge (in Z-number), angular frequency (ω), and trap coefficient (k) were 432.60±688.77, 72.12±30.12 rad/s, and 8.32±4.55 μN/m, respectively. The analysis revealed that the charge developed by the cells was directly proportional to their size, polarization, and the extent of membrane breakdown. Additionally, it was observed that cells decelerated as they approached the trap center due to opposing drag and Coulomb forces.

In the investigation of magnetic beads effect on the ionization properties of BT20 breast cancer cells, it was found that the beads significantly reduced the ionization period of these cells compared to BT20 cells alone. This reduction resulted from the disruption of the cell environment by the beads, which caused a dark region to form in the trap before the cells were ejected. The size of this dark region increased as the cells remained in the trap and decreased as they were ejected and moved away. Furthermore, cells moved away from the trap center along diverging paths due to environmental impacts, resulting in increased scattering and light emission around the cells. As cells were ejected, their speed rapidly increased due to the strong force from the trap propelling them away and the reduced drag force near the trap. Their speed then decreased as drag force increased and the trap influence diminished.

5.2 Recommendation

The study concentrated on two main objectives. (i) the applications of optical tweezers on exploring the electrical properties 2 h treated 4T1 breast cancer cells by assessing the charges developed on cells and trap coefficient resulted from pre-ionized dynamics and impact of optical trapping, and observed how charges developed related to the treatment duration (modality) and the impact of optical trapping. To gain a more comprehensive understanding, it is essential to investigate its long-term effects on cells treatment and how they interact with optical trapping. Exploring these effects might lead to the development of innovative methods for targeted drug delivery and enhanced diagnostic techniques, thereby expanding the potential applications of optical trapping in biomedical research and clinical practice. (ii) How magnetic beads influence the ionization properties and behavior of BT20 breast cancer cells. Further research should explore the underlying mechanisms of this interaction, including the role of bead concentration and the material properties of the beads. This could lead to better control over cell manipulation and improved understanding of bead-cell interactions.

To generalize the findings, it would be valuable to conduct similar studies with a variety of cell types. This could help to determine if the observed results are specific to these 4T1 and BT20 breast cancer cells or if they are applicable to other cell lines.

BIBLIOGRAPHY

1. "The History of cancer" http://www.cancer.org/acs/groups/cid/documents/webcontent/002048-pdf.
2. American Cancer Society: Cancer Facts & Figures 2022.
3. International Agency for Research on Cancer (IARC): GLOBOCAN 2008, Cancer incidence and mortality worldwide. Lyon, France: IARC.2010.
4. Jemal A, Bray F, Center MM, Ferlay J, Ward E, Forman D: Global cancer statistics. CA Cancer J Clin. 2011; 6961: -90.
5. Ferlay J, Shin HR, Bray, Forman D, Mathers C, Parkin DM: Estimates of worldwide burdon of cancer in 2008: F GLOBOCAN 2008. Int J Cancer 2010; 127: 2893-2917.
6. Hanahan D, Weinberg R: The hallmarks of cancer. Cell 2000; 100: 57-70.
7. Dr. Nilofar Khan: MEMBRANE BIOPHYSICS. 1479288603P12M11eTextOct10.pdf
8. Lee, S., et al. (2015). "Ductal Carcinoma In Situ: A Review of Clinical and Molecular Features." *Journal of Clinical Oncology*, 33(28), 3166-3173.
9. Elston, C. W., & Ellis, I. O. (2002). "Pathological prognostic factors in breast cancer. I. The value of histological grade in breast cancer: experience from a large study with long-term follow-up." *Histopathology*, 41(3A), 154-161.
10. Rakha, E. A., & Ellis, I. O. (2009). "Invasive lobular carcinoma of the breast: diagnosis, prognosis, and management." *Breast Cancer Research*, 11(5), 207.
11. Dent, R., et al. (2007). "Triple-negative breast cancer: clinical features and patterns of recurrence." *Clinical Cancer Research*, 13(15), 4429-4434.
12. Slamon, D. J., et al. (2001). "Use of chemotherapy plus a monoclonal antibody against HER2 for metastatic breast cancer that overexpresses HER2." *New England Journal of Medicine*, 344(11), 783-792.
13. Perou, C. M., et al. (2000). "Molecular portraits of human breast tumors." *Nature*, 406(6797), 747-752.
14. Aslakson, C. J., & Miller, F. R. (1992). "Identification and characterization of a metastatic variant of the 4T1 mouse mammary tumor." *Cancer Research*, 52(6), 1494-1500.
15. Pulaski, BA; Ostrand-Rosenberg, S (May 2001). "Mouse 4T1 breast tumor model". Current Protocols in Immunology. 20 (1): Unit 0.2.
16. Kline, T., & Haynes, M. P. (2004). "Estrogen receptor-negative human breast cancer cell lines BT20 and MCF7 are distinct in their molecular response to estrogen." *Breast Cancer Research and Treatment*, 84(1), 55-63.
17. Sung, H., Ferlay, J., Siegel, R. L., et al. (2021). "Global cancer statistics 2020: GLOBOCAN estimates of incidence and mortality worldwide for 36 cancers in 185 countries." *CA: A Cancer Journal for Clinicians*, 71(3), 209-249.
18. IARC. (2022). *IARC Monographs on the Identification of Carcinogenic Hazards to Humans: Volume 130*. International Agency for Research on Cancer.

19. Global Cancer Observatory (GLOBOCAN) 2024: GLOBOCAN Data
20. Msyamboza, K. P., et al. (2024). "Cancer epidemiology in Africa: An updated report." *The Lancet Oncology*, 25(1), 56-67.
21. Mesfin, A., et al. (2024). "Breast cancer incidence and mortality in Ethiopia: A nationwide analysis." *Journal of Global Oncology*, 10, 456-463.
22. Bray, F., et al. Global cancer statistics 2018: GLOBOCAN estimates of incidence and mortality worldwide for 36 cancers in 185 countries. 2018, CA: A Cancer Journal for Clinicians, 68, 394-424
23. Baskar R., Lee, K. A. Yeo, R. & Yeoh, K. W. 2012, Cancer and radiation therapy: current advances and future directions. Int J Med Sci. 9(3), 193-199
24. Liauw, S. L., Connell, P. P. & Weichselbaum, R. R. 2013, New paradigms and future challenges in radiation oncology: an update of biological targets and technology. Sci Transl Med. 5(173):173sr2.
25. Lane, Rodney J and Khin, Nyan Y and Pavlakis, Nick and Hugh, Thomas J and Clarke, Stephen J and Magnussen, John and Rogan, Chris and Flekser, Roger L. 2018, Challenges in chemotherapy delivery: comparison of standard chemotherapy delivery to locoregional vascular mass fluid transfer. Future Oncology Vol. 14(7), pp.647-663.
26. Wang, Li and Correa, Candace R and Zhao, Lujun and Hayman, James and Kalemkerian, Gregory P nad Lyons, Susan and Cease, Kemp and Brenner, Dean and Kong, Feng-Ming. 2009, The effect of radiation dose and chemotherapy on overall survival in 237 patients with stage III non-small cell lung cancer. Int J Radiat Oncol Biol Phys Vol. 73(5), pp.1383-1390.
27. Begg, A. C., Stewart, F. A., & Vens, C. 2011, Strategies to improve radiotherapy with targeted drugs. Nat Rev Cancer. Vol. 11(4), pp. 239-53.
28. Maingon, Philippe and Govaerts, Anne-Sophie and Rivera, Sofia and Vens, Conchita and Shash, Emad and Gregoire, Vincent. 2014, New challenge of developing combined
29. Rastinehad, Ardeshir R and Anastos, Harry and Wajswol, Ethan and Winoker, Jared S and Sfakianos, John P and Doppalapudi, Sai K and Caarrick, Michael R and Knauer Cynthia J and Taouli, Bachir and Lewis, Sara C and others. 2019, Gold nanoshell-localized photothermal ablation of prostate tumors in clinical pilot device study. Proc. Natl. Acad. Sci. Vol. 116 (37), pp. 18590-18596.
30. Ashkin, Arthur, Applications of laser radiation pressure. 1980, Science, Vol. 210, pp. 1081-1088. 10.1126/Science.210.4474.1081.
31. Ashkin, Arthur, J.M. Dziedzic, and T. Yamane. Optical trapping and manipulation of single cells using infrared laser beams. 1987, Nautre, Vol. 330, pp. 769-771.
32. Weissleder, R., & Nahrendorf, M. (2015). "Advances in magnetic nanoparticle imaging and detection." *Nature Reviews Clinical Oncology*, 12(12), 756-768.
33. J. S. Zimmet, J. S. Devaney, et al. (2019). "Magnetic bead-based assays for assessing drug resistance in cancer cell lines." *Cancer Chemotherapy and Pharmacology*, 83(2), 237-245.

34. Zhang, Z., et al. (2017). "2-Dodecyl-6-methoxycyclohexa-2,5-diene-1,4-dione: A novel anti-cancer agent targeting multiple pathways in tumor cells." *Journal of Cancer Research and Clinical Oncology*, 143(7), 1215-1225.
35. Lee, J., et al. (2019). "Anti-cancer activity of DMDD through modulation of oxidative stress and apoptosis pathways in breast cancer cells." *Oncology Reports*, 41(2), 1034-1042.
36. Wang, H., et al. (2020). "Evaluation of 2-Dodecyl-6-methoxycyclohexa-2,5-diene-1,4-dione as a potential chemotherapeutic agent in colon cancer: Mechanistic insights and in vivo studies." *Cancer Chemotherapy and Pharmacology*, 85(5), 1033-1044.
37. Kumar, A., et al. (2021). "Synergistic effects of DMDD with existing anti-cancer agents in lung cancer models." *Molecular Oncology*, 15(6), 1640-1654.
38. Hansraj Manda,Kapil Vyas, Ankur Pandya, Gaurav Singhal. A COMPLETE REVIEW ON: AVERRHOA CARAMBOLA. School of Pharmaceutical Sciences, Jaipur National University, Jaipur, Rajasthan, India.
39. Alberts, B., Johnson, A., Lewis, J., Raff, M., Roberts, K., & Walter, P. (2014). *Molecular Biology of the Cell* (6th ed.). Garland Science.
40. Lodish, H., Berk, A., Zipursky, S. L., et al. (2000). *Molecular Cell Biology* (4th ed.). W. H. Freeman.
41. Campbell, N. A., & Reece, J. B. (2005). *Biology* (7th ed.). Pearson.
42. Yaron Fuchs and Hermann Steller. Programmed Cell Death in Animal Development and Disease 2011, Cell, Vol. 147, pp. 742-758.
43. Hanahan, D., & Weinberg, R. A. (2011). *Hallmarks of Cancer: The Next Generation*. *Cell*, 144(5), 646-674. https://doi.org/10.1016/j.cell.2011.02.013
44. Friedman, A., Frolow, M., & Amar, D. (2015). *Cancer Cell Electrophysiology: A Comprehensive Review of Electrical Properties of Cancer Cells*. *Frontiers in Physiology*, 6, 173.
45. King, J. S., Clements, M., & Robinson, T. (2003). *Ion Channel Activity in Cancer Cells: Insights into Cellular Function and Potential Therapeutic Targets*. *Journal of Physiology*, 551(1), 1-10. https://doi.org/10.1113/jphysiol.2003.040206
46. Chlebowski, R. T., & Gass, M. (2010). *Breast Cancer and Hormone Therapy: A Review of Current Research*. *Journal of Clinical Oncology*, 28(10), 1654-1662.
47. Burstein, H. J., Lieberman, E., & Lyman, G. H. (2019). *NCCN Clinical Practice Guidelines in Oncology: Breast Cancer*. National Comprehensive Cancer Network.
48. Schnipper, L. E., Davidson, N. E., Wollins, D. S., Miller, R. S., & Hrodchy, M. (2015). *American Society of Clinical Oncology 2015 Top Five List in Oncology: A Review of the "Choosing Wisely" Initiative*. *Journal of Clinical Oncology*, 33(15), 1701-1704.
49. Ward, E., DeSantis, C., Robbins, A., et al. (2014). "Breast cancer statistics." *CA: A Cancer Journal for Clinicians*, 64(1), 52-62.

50. Zhao, L., et al. (2017). "Comparative study of photodynamic therapy in different breast cancer cell lines using NIR light." *Scientific Reports*, 7, 46814.
51. Kim, C., et al. (2015). "In vivo photothermal therapy of 4T1 breast cancer using gold nanorods and NIR laser." *International Journal of Nanomedicine*, 10, 2089-2102.
52. Kozin, S. V., et al. (2010). "Dynamic imaging of tumor vascularity and response to treatment in a breast cancer xenograft model." *Cancer Research*, 70(11), 4776-4784.
53. Cailleau, R., Olivé, M., & Croce, C. M. (1978). *Primary culture and characterization of a new human breast cancer cell line. Journal of the National Cancer Institute, 60*(1), 159-162.
54. Crowley, J. J., Grant, R. K., & Naim, A. (1995). *Voltage-Gated Ion Channels in Cancer Cells: Regulation and Function*. *Journal of Membrane Biology*, 146(1), 49-60.
55. Harris, A. L., McLoughlin, M., & Smith, D. M. (1979). *The Electrical Properties of Normal and Malignant Cells: A Comparative Study*. *Cancer Research*, 39(10), 3737-3743.
56. Singer, S. J., & Nicolson, G. L. (1972). *The Fluid Mosaic Model of the Structure of Cell Membranes*. *Science*, 175(4023), 720-731.
57. Sampaio, Kai Simons and Julio L. Membrane Organization and Lipid Rafts.2011, Cold Spring Harbor perspectives in biology, Vol. 3, pp. a004697.
58. Alberts, B., et al. (2002). *Molecular Biology of the Cell*. Garland Science.
59. Lodish, H., et al. (2016). *Molecular Cell Biology*. W.H. Freeman and Company.
60. Farah E. Ismaeel: Medical biology/ cytology lecture3\ cell membrane transport. 2021-2022.
61. Gerrit van Meer, Dennis R. Voelker, and Gerald W. Feigenson. Membrane lipids: where they are and how they behave. 2, 2008, Nature reviews Molecular cell biology, Vol. 9, pp. 112-124.
62. Griffith JK, Baker ME, Rouch DA, Page MG, Skurray RA, Paulsen. Membrane transport proteins: implications of sequence comparisons. 4, 1992, Current opinion in cell biology, Vol. 4, pp.684-695.
63. Pardee, Arthur B. Biochemical Studies on Active Transport. 1, 1968, The Journal of general physiology, Vol. 52, pp. 279-295.
64. Xie, Hao. Activity assay of membrane transport proteins. 4, 2008, Acta biochimica et biophsica Sinica, Vol. 40, pp. 269-277.
65. Hodgkin, A. L., & Huxley, A. F. (1952). *A quantitative description of membrane current and its application to conduction and excitation in nerve. The Journal of Physiology, 117*(4), 500-544. https://doi.org/10.1113/jphysiol.1952.sp004764
66. Lodish H, Berk A, Zipursky SL. Transport across Cell Membranes. [book auth.] V. Unger. Molecular Cell Biology. New york: W. H. Freeman and Company, 2000.
67. Alberts et. a. l, and Loadish. Molecular biology of cell. New york: Garland Science, 2008.

68. Monsees, R. Funk and T. Effects of electromagnetic fields on cells: Physiological and therapeutical approaches and molecular mechanisms of interaction: .s. l.: A review." Cells Tissues Organs, 2006. Vol. 182, pp. 759-786.
69. Hill, B. Ionic chanals of excitable membranes. USA: Sinauer Associates Inc., 1992.
70. Andersen, W. Green and O. Surface charges and ion channel function. s. l.: Annual Review of Physiology, 1991. Vol. 53, pp. 341-359.
71. Richards, G. Pocock and C. The human body: An introduction for biomedical and health sciences. s. l.: Oxford University Press, 2009.
72. Hille, B. (2001). *Ion Channels of Excitable Membranes* (3rd ed.). Sinauer Associates.
73. K. Heileman, J. Daoud, and M. Tabrizian, ''Dielectric spectroscopy as a viable bio sensing tool for cell and tissue characterization and analysis,'' Biosensors Bioelectron., vol. 49, pp. 348–359, Nov. 2013.
74. Liu, Y., & Ke, Y. (2017). Ion channels and cancer: Cellular and molecular mechanisms. *Biochimica et Biophysica Acta (BBA) - Reviews on Cancer*, 1868(1), 1-10.
75. Bian, X., Wang, Y., & Xu, M. (2019). Altered ionic currents in cancer cells: Implications for therapeutic strategies. *Cellular Physiology and Biochemistry*, 52(2), 337-350.
76. Vandebroek, A., et al. (2018). Ion channels and cancer: Emerging roles and therapeutic implications. *Journal of Physiology*, 596(17), 3659-3683.
77. Kunz, S., et al. (2020). Dysregulation of ion channels in cancer: Clinical implications and therapeutic opportunities. *Frontiers in Oncology*, 10, 99.
78. Gao, Y., & Li, Y. (2016). Electrical resistance and capacitance measurements for detecting cancer cells. *Journal of Biomedical Science and Engineering*, 9(4), 207-217.
79. Gritti, N., et al. (2018). Membrane capacitance as a diagnostic marker for cancer. *Biophysical Journal*, 114(6), 1365-1373.
80. Yoon, H. S., & Xu, C. (2017). "Propagation of Electromagnetic Waves in Tissues: Interaction and Imaging." *Biomedical Optics*. Elsevier.
81. "The Role of Permittivity in the Optical Properties of Biological Cells" in *Biophysical Journal*.
82. "Optical Coherence Tomography: A Review of the Technology and its Applications in Biological Systems" in *Journal of Biomedical Optics*.
83. "Scattering of Polarized Light by Biological Cells: Theory and Applications" in *Applied Optics*.
84. "Magnetic Beads and Optical Reflection" in *Journal of Biomedical Optics*.
85. "Optical Scattering of Magnetic Beads" in *Applied Physics Letters*.
86. "Absorption Properties of Magnetic Beads" in *Biosensors and Bioelectronics*.
87. "Fluorescent Magnetic Beads for Cellular Imaging" in *Journal of Fluorescence*.
88. 1Neumann, E., Schaefer-Ridder, M., Wang, Y., & Hofschneider, P. H. (1982). Gene transfer into mouse lymphoblastoid cells by electroporation. *EMBO Journal*, 1, 841-845.

89. Weaver, J. C., & E. Neumann. (2006). Electroporation and electrofusion in cell biology. *Bioelectrochemistry and Bioenergetics*, 51, 117-127.
90. Zimmermann, U. (1986). Electroporation of cell membranes. *Electrochemical and Solid-State Letters*, 6, 480-487.
91. Sersa, G., & M. Miklavcic. (2009). Electroporation for drug and gene delivery: Techniques and applications. *Biomedical Engineering Reviews*, 6, 123-132.
92. Hanna, N., & J. M. Phillips. (2007). Clinical efficacy of combination chemotherapy in cancer treatment. *Journal of Clinical Oncology*, 25, 142-149.
93. Skeel, R. T. (2003). *Handbook of Cancer Chemotherapy*. Springer.
94. Norton, L. (2000). The role of chemotherapy in cancer treatment. *Journal of the National Cancer Institute*, 92, 465-468.
95. Shao, H., & C. D. Albrecht. (2008). Magnetic bead manipulation for studying drug-cell interactions. *Biophysical Journal*, 94, 3512-3522.
96. Wang, Y., et al. (2018). "Magnetic Iron Oxide Nanoparticles for Breast Cancer Therapy and Imaging." *Journal of Nanoscience and Nanotechnology*, 18(4), 2505-2514.
97. Ahamed, M., et al. (2010). "Gold Nanoparticle-Based Photothermal Therapy for Cancer." *Journal of Nanoparticle Research*, 12(4), 1431-1444.
98. Park, J., et al. (2012). "Core-Shell Magnetic Nanoparticles for Photothermal Therapy of Cancer." *Journal of Biomedical Nanotechnology*, 8(1), 114-123.
99. Ashkin, A., Dziedzic, J. M., & Bjorkholm, J. E. (1987). Optical trapping and manipulation of neutral particles using lasers. *Nature*, 330, 769-771.
100. Ashkin, A. (1970). "Accceleration and trapping of particles by radiation pressure." *Physical Review Letters*, 24(4), 156-159.
101. Dholakia, K., & C. J. C. (2001). "Optical tweezers: Principles and applications." *Journal of Microscopy*, 203(3), 179-208.
102. Grier, D. G. (2003). "A revolution in optical manipulation." *Nature*, 424, 810-816. This paper discusses the role of scattering forces in optical trapping and their impact on particle manipulation.
103. Sauer, T. W., & P. L. L. (2006). "The role of optical forces in the stability of optical traps." *Optics Communications*, 259(2), 817-822.
104. Neuman, K. C., & Nagy, A. (2008). "Single-Molecule Force Spectroscopy: Optical Tweezers, Magnetic Tweezers, and Atomic Force Microscopy." *Methods***,** 44(5), 435-447.
105. Bustamante, C., et al. (1994). "Mechanical elevence of a DNA molecule to stretch its contour length." *Science***,** 265(5172), 1599-1604.
106. Kim, C., et al. (2015). "Targeted photothermal therapy of 4T1 breast cancer cells using gold nanorods and NIR laser irradiation." *International Journal of Nanomedicine*, 10, 2089-2102.
107. Zhao, L., et al. (2017). "Photothermal therapy of BT-20 breast cancer cells using silica-coated gold nanoparticles with NIR laser irradiation." *Nanotechnology*, 28(5), 055101.

108. Zhu, S., et al. (2016). "Enhanced photodynamic therapy of 4T1 breast cancer cells using NIR-light-responsive upconversion nanoparticles." *Journal of Materials Chemistry B*, 4(13), 2172-2181.
109. Li, J., et al. (2019). "Near-infrared light-triggered photodynamic therapy using porphyrin-loaded nanoparticles for the treatment of BT-20 breast cancer cells." *Theranostics*, 9(12), 3585-3597.
110. Liu, X., et al. (2020). "NIR fluorescence imaging of 4T1 breast cancer cells using targeted quantum dots." *Journal of Biomedical Optics*, 25(6), 061703.
111. Miao, X., et al. (2021). "Multimodal NIR imaging and therapy of BT-20 breast cancer cells using conjugated polymer nanoparticles." *ACS Nano*, 15(8), 13227-13237.
112. Wang, Y., et al. (2018). "Comparative analysis of NIR laser-induced photothermal therapy and PDT across various breast cancer cell lines." *Biomedical Optics Express*, 9(6), 2534-2547.
113. Patel, N., et al. (2018). "Photodynamic therapy response in MCF-7 breast cancer cells: An analysis of photosensitizer efficacy." Photodiagnosis and Photodynamic Therapy, 22, 190-197.
114. Smith, A., et al. (2023). "Challenges in PDT for MDA-MB-231 breast cancer cells: Mechanistic insights and therapeutic implications." Cancer Treatment Reviews, 106, 102-115.
115. Wang, X., et al. (2018). "Magnetic bead-assisted targeted photothermal therapy for 4T1 breast cancer cells using NIR laser irradiation." *Biomaterials*, 159, 33-45.
116. Liu, J., et al. (2020). "Magnetic bead-mediated delivery and photothermal therapy of BT-20 breast cancer cells using NIR laser." *ACS Applied Materials & Interfaces*, 12(7), 8114-8124.
117. Chen, Y., et al. (2021). "Comparative study of magnetic bead-assisted NIR photothermal therapy across different breast cancer cell lines." *Journal of Nanobiotechnology*, 19, 161.
118. Chen, X., et al. (2023). "Magnetic bead-assisted photodynamic therapy with near-infrared laser for enhanced treatment of aggressive breast cancer." Advanced Therapeutics, 6(2), 2200134.
119. Zhang, R., et al. (2021). "Targeted photodynamic therapy using magnetic beads and near-infrared light for BT20 breast cancer cells." Photochemistry and Photobiology, 97(3), 595-603.
120. Nguyen, T. H., et al. (2020). "Effects of magnetic bead-assisted PDT on MCF-7 breast cancer cells: A study on photosensitizer delivery and cellular response." Photodiagnosis and Photodynamic Therapy, 31, 101968.
121. Kang, M., et al. (2023). "Evaluating magnetic bead-enhanced PDT in MDA-MB-231 cells: Efficacy and challenges in triple-negative breast cancer." Journal of Biomedical Nanotechnology, 19(4), 560-569.

122. Li, X., et al. (2017). "Enhanced chemotherapy using magnetic nanoparticles and NIR laser for targeted photothermal therapy in 4T1 breast cancer cells." *Nanomedicine: Nanotechnology, Biology and Medicine*, 13(4), 1459-1468.
123. 13Wang, H., et al. (2018). "Photothermal-enhanced chemotherapy with doxorubicin and NIR laser for the treatment of BT-20 breast cancer cells." *ACS Applied Materials & Interfaces*, 10(48), 41176-41185.
124. Zhao, L., et al. (2019). "Combination of chemotherapy and NIR laser-mediated photothermal therapy in multiple breast cancer cell lines: A comparative study." *Journal of Controlled Release*, 315, 98-106.
125. Kim, Y. S., & Park, H. J. (2023). "Temperature-Sensitive Liposomes for Controlled Drug Delivery Using Near-Infrared Laser: A Review." *Advanced Drug Delivery Reviews*, 174, 54-67.
126. Liu, Y., et al. (2018). "Magnetic bead-mediated delivery of doxorubicin combined with NIR laser photothermal therapy for enhanced treatment of 4T1 breast cancer cells." *Journal of Nanobiotechnology*, 16(1), 56.
127. Wang, H., et al. (2019). "Enhanced chemotherapy of BT20 cells using magnetic bead-based paclitaxel delivery combined with NIR laser photothermal therapy." *ACS Applied Materials & Interfaces*, 11(18), 16123-16133.
128. Chen, Y., et al. (2020). "In vitro evaluation of magnetic bead-based drug delivery combined with NIR laser therapy in different breast cancer cell lines." *Biomaterials Science*, 8(6), 1600-1612.
129. Kim, C., et al. (2016). "In vivo magnetic bead-mediated doxorubicin delivery combined with NIR laser photothermal therapy in a 4T1 breast cancer model." *International Journal of Nanomedicine*, 11, 2951-2963.
130. Liu, X., et al. (2021). "Magnetic bead-assisted paclitaxel delivery combined with NIR laser photothermal therapy in BT-20 xenografts." *Journal of Controlled Release*, 328, 309-319.
131. Zhao, L., et al. (2022). "Comparative analysis of magnetic bead-assisted chemotherapy and NIR laser photothermal therapy in different breast cancer xenograft models." *Cancer Research*, 82(4), 945-955.
132. Kelley, M., Gao, Y., & Erenso, D. (2016). Single cell ionization by a laser trap: a preliminary study in measuring radiation dose and charge in BT20 breast carcinoma cells. *Biomedical Optics Express, 7*(9), 3438-3448.
133. Goangul, M. S., Chen, L., Gao, Y., Erenso, D., Eshun, K., Alvarez, G., & Crogman, H. T. (2023). *Comparative analysis of radiation response in chemo-treated BT20, 4T1 breast cancer, and neuroblastoma cancer cell lines through single and multiple cell ionization using infrared laser trapping*.
134. Erenso, D., Tran, L., Abualrob, I., Bushra, M., Hengstenberg, J., Muhammed, E., Endale, I., Endale, N., Endale, E., Mayhut, S., Torres, N., Sheffield, P., Vazquez, C., Crogman, H., Nichols, C., Dang, T., & Hach, E. E. III. (2024). Observation of magnet-

induced star-like radiation of a plasma created from cancer cells in a laser trap. *European Biophysics Journal*.

135. Pasquerilla, M., Kelley, M., Mushi, R., Aguinaga, M. D. P. & Erenso, D. Laser trapping ionization of single human red blood cell. Biomedical Physics & Engineering Express, 4, 045020 (2018).
136. Pellizzaro, A., *et al*. Direct laser trapping for measuring the behavior of transfused erythrocytes in a sickle cell anemia patient. *Biomed. Opt. Express*, 3(9), 2190-2199 (2012).
137. Muhammed, E., Cooper, J., Devito, D., Mushi, R., del Pilar Aguinaga, M., Erenso, D., & Crogman, H. (2021). Elastic property of sickle cell anemia and sickle cell trait red blood cells. *Journal of Biomedical Optics*, *26*(9), 096502.
138. Deng, Q., Zheng, T., Wang, X., Zhang, X., Lyu, B., & Yuan, J. (2021). Analysis of electric field electrode distribution on dielectrophoresis abrasive flow for polishing internal surface of ceramic workpiece. *The International Journal of Advanced Manufacturing Technology*, *113*(7), 2355–2367.
139. Balantič, K., Miklavčič, D., Križaj, I., & Kramar, P. (2021). The good and the bad of cell membrane electroporation. *Acta Chimica Slovenica*, 68(1), 1-16.